

# Quantum Power Iteration Unified Using Generalized Quantum Signal Processing

Viktor Khinevich,<sup>1,2,\*</sup> Yasunori Lee,<sup>3</sup> Nobuyuki Yoshioka,<sup>4</sup> and Wataru Mizukami<sup>1,2,†</sup>

<sup>1</sup>*Graduate School of Engineering Science, Osaka University,*

*1-3 Machikaneyama, Toyonaka, Osaka 560-8531, Japan*

<sup>2</sup>*Center for Quantum Information and Quantum Biology,  
Osaka University, 1-2 Machikaneyama, Toyonaka 560-8531, Japan*

<sup>3</sup>*QunaSys, 1-13-7 Hakusan, Bunkyo-ku, Tokyo 113-0001, Japan*

<sup>4</sup>*International Center for Elementary Particle Physics, The University  
of Tokyo, 7-3-1 Hongo, Bunkyo-ku, Tokyo 113-0033, Japan*

We present a unifying framework for quantum power-method-based algorithms through the lens of generalized quantum signal processing (GQSP): we apply GQSP to realize quantum analogues of classical power iteration, power Lanczos, inverse iteration, and folded spectrum methods, all within a single coherent framework. Our approach is efficient in terms of the number of queries to the block encoding of a Hamiltonian. Also, our approach can avoid Suzuki–Trotter decomposition. We constructed quantum circuits for GQSP-based quantum power methods, estimated the number of queries, and numerically verified that this framework works. We additionally benchmark various quantum power methods with molecular Hamiltonians and demonstrate that Quantum Power Lanczos converges faster and more reliably than standard Quantum Power Iteration, while Quantum Inverse Iteration outperforms existing inverse iteration variants based on time-evolution operators. We also show that the Quantum Folded Spectrum Method can obtain excited states without variational optimization. Overall, our results indicate that GQSP-based implementations of power methods combine scalability, flexibility, and robust convergence, paving the way for practical initial state preparations on fault-tolerant quantum devices.

## I. INTRODUCTION

Quantum computing has been developing rapidly, driven by advances in both hardware architectures and algorithmic design. Quantum computers are widely believed to outperform classical ones in condensed matter physics, quantum chemistry, and materials science [1, 2]. A key computational challenge in these domains is to solve the eigenvalue problem.

The most direct method of finding eigenvalues on a quantum computer is the quantum phase estimation (QPE) algorithm [3, 4]. Despite its conceptual elegance, QPE typically requires substantial computational resources, demanding fault-tolerant quantum computers (FTQCs). Even proposals to reduce its overhead [5, 6] face the fundamental challenge of preparing a high-fidelity initial state of the target state.

A widely used algorithm to prepare an approximate quantum state is the variational quantum eigensolver (VQE) [7], which utilizes a hybrid quantum-classical approach. VQE offers the advantage of shallow circuits compatible with existing hardware [8–10]. However, its reliance on classical optimization makes it vulnerable to issues such as barren plateaus [11], limiting the scalability for more expressive ansatzes.

Imaginary-time evolution (ITE) offers another route to ground state preparation by approximating the non-unitary propagator [12]. While classical ITE has

long been a workhorse for quantum many-body simulations, quantum adaptations face their own challenges. Many implementations inherit Trotter errors of time-evolution [13–15], high resource costs to estimate the quantum Fisher information matrix [16], or post-selection overheads [17]. Moreover, ITE is naturally tailored to find ground states, which limits its versatility for broader classes of problems.

In contrast, power methods represent a more general and flexible family of iterative algorithms with a long history of use in classical numerical linear algebra. Beyond ground-state preparation, power methods include algorithms for computing excited states, inverting matrices, solving linear systems, and performing principal component analysis. Because of this, they are widely used in many areas, such as computer-aided engineering, finance, and machine learning. Adapting these versatile techniques to quantum computers offers the promise of broadly useful linear-algebraic building blocks for scientific and industrial applications.

Recent work has explored various ways of implementing quantum power methods. Techniques include linear combinations of unitaries (LCU) to implement powers of cosine transformed Hamiltonians [18], finite-difference approximations of time evolution operators [19], direct encoding using rotational operators [20], HHL-based approach [21, 22] and singular value transformation (QSVT) [23–25]. Similarly, inverse iteration schemes were also implemented [26–29]. Krylov subspace methods [30–32] extend these ideas to more sophisticated approaches. However, many of these implementations face practical limitations, such as Trotter errors, high qubit costs, and restrictions to only real-valued polynomials.

\* victorkh711@gmail.com

† mizukami.wataru.qiqb@osaka-u.ac.jp

This study demonstrates that various power methods can be implemented in a unified way using generalized quantum signal processing (GQSP) [33] (or more specifically generalized quantum singular value transformation (GQSVT) [34]). The main advantage of GQSP over QSP is that it can encode any general complex polynomial without additional overhead. This paves the way for implementation of the power Lanczos method, which may require complex coefficients, and also for future development of Green's function and complex energy shifts in the inverse iteration method. Moreover, the GQSP gives advantage over methods that use a linear combination of time-evolution operators. For example, our implementation of the quantum inverse iteration is free of Trotter error and requires fewer qubits in numerical tests than the existing approaches.

Additionally, using the same technique, we introduced the quantum folded spectrum method for calculating excited states. Before, this method was used in the VQE framework, which required explicit construction of a Hamiltonian squared. That leads to measurements of a large number of terms [35]. GQSP allows us to avoid explicit construction of powers of Hamiltonian and variational optimization.

We constructed quantum circuits and numerically verified that this approach works. In addition, we investigated the number of queries and the practical qubit count. Note that our methods are essentially equivalent to classical computation methods and can be executed classically if an exponential amount of memory is available. However, the power iteration methods implemented in this paper have not been used in quantum chemistry calculations, so limited data is available. For this reason, we also verified the convergence behavior of the power method used.

The remainder of this paper is organized as follows. Section II reviews the fundamentals of GQSP and presents our implementations of various power methods. In Section III computational details are presented. Section IV then provides numerical verification of our methods and compares them with existing approaches, focusing on their convergence performance for model Hamiltonians and their respective computational costs. Finally, Section V summarizes our findings, discusses potential improvements, and presents directions for further research and development.

## II. THEORY

### A. Generalized quantum signal processing (GQSP)

QSP is a powerful framework to efficiently implement polynomial transformations of a Hermitian operator  $H$  [36]. The operator  $H$  is first embedded in a larger unitary operator  $U$  using a block encoding procedure. This encoding is sufficiently general to represent not only Hermitian operators but also non-Hermitian ones, laying

the foundation for the more comprehensive framework of QSVT [23]. The first distinction between GQSP and conventional QSP techniques is the form of the signal operator. Instead of employing  $R_x$  or  $R_z$  rotations, GQSP uses a 0-controlled block encoding operator, denoted by  $CU_0$ . This operator is defined as

$$CU_0 = (|0\rangle\langle 0| \otimes U) + (|1\rangle\langle 1| \otimes I) = \begin{pmatrix} U & 0 \\ 0 & I \end{pmatrix}, \quad (1)$$

where  $U$  is the block encoding operator.

The second key difference is that, rather than restricting the rotations to  $R_x$  or  $R_z$ , GQSP employs general  $SU(2)$  rotation operators on the auxiliary qubit. These rotations are defined as

$$R(\theta, \phi, \lambda) = \begin{bmatrix} e^{i(\lambda+\phi)} \cos(\theta) & e^{i\phi} \sin(\theta) \\ e^{i\lambda} \sin(\theta) & -\cos(\theta) \end{bmatrix}. \quad (2)$$

Moreover, except for the first rotation, the parameter  $\lambda$  can be set to zero without loss of expressivity.

**Theorem 1 (Generalized Quantum Signal Processing [33])** *Let  $U$  be a unitary operator. Then there exist angles  $\vec{\theta} = (\theta_0, \theta_1, \dots, \theta_d)$  and  $\vec{\phi} = (\phi_0, \phi_1, \dots, \phi_d)$  in  $\mathbb{R}^{d+1}$ , along with a phase parameter  $\lambda \in \mathbb{R}$ , such that*

$$\begin{pmatrix} P(U) & * \\ Q(U) & * \end{pmatrix} = \left( \prod_{j=1}^d R(\theta_j, \phi_j, 0) CU_0 \right) R(\theta_0, \phi_0, \lambda), \quad (3)$$

*if and only if the following conditions hold:*

1.  $P, Q \in \mathbb{C}[z]$  satisfying  $\deg(P), \deg(Q) \leq d$ .
2.  $\forall z \in \mathbb{C}$  with  $|z| = 1$ , the relation

$$|P(z)|^2 + |Q(z)|^2 = 1$$

*holds.*

The quantum circuit corresponding to this theorem is shown in Fig. 1. The polynomial transformation  $P(U)$  is achieved by sandwiching the signal operators  $U$  with the signal processing operators.

The central challenge of the GQSP method is to determine the angle sequences  $\vec{\theta}$ ,  $\vec{\phi}$ , and the phase parameter  $\lambda$  that produce the desired polynomial  $P(z)$ . As a first step, for any target polynomial  $P(z)$ , one must construct a complementary polynomial  $Q(z)$  that satisfies  $|P(z)|^2 + |Q(z)|^2 = 1$  for all  $z$  on the complex unit circle. It has been rigorously proven that this complementary polynomial exists for any  $P(z)$  with  $|P(z)| \leq 1$  for all  $z \in \mathbb{T}$  [33]. Various methods exist to determine the appropriate angles; further details are discussed in the Appendix B.

In this paper, we focus exclusively on GQSP of Hamiltonians of multiqubit systems and adopt the corresponding terminology throughout the text. More generally, the

exact same GQSP framework carries over to any diagonalizable operator. Hamiltonians are merely a particularly nice example, offering well-studied block encoding constructions and physically motivated initial guesses.

The Hamiltonian  $H$  can be block encoded into a unitary operator  $U$ . Specifically, we define

$$U = \begin{pmatrix} \mathcal{H} & \mathcal{A} \\ \mathcal{B} & \mathcal{C} \end{pmatrix}, \quad (4)$$

where  $\mathcal{H} = H/\|H\|_{\ell_1}$ . Here,  $\|H\|_{\ell_1}$  is the LCU norm: if one writes  $H = \sum_k \alpha_k P_k$  as a linear combination of Pauli terms  $P_k$ , then  $\|H\|_{\ell_1} = \sum_k |\alpha_k|$ . The off-diagonal blocks  $\mathcal{A}$  and  $\mathcal{B}$  are generically rectangular isometries because the ancilla dimension does not need to match that of the Hamiltonian.

The unitarity of  $U$  implies the following relations:

$$\mathcal{A}\mathcal{A}^\dagger = \mathcal{B}^\dagger\mathcal{B} = I - \mathcal{H}^2. \quad (5)$$

Because  $(I - \mathcal{H}^2)$  is positive semi-definite, we can apply a polar decomposition to the off-diagonal blocks:

$$\begin{aligned} \mathcal{A} &= V\sqrt{\mathcal{A}\mathcal{A}^\dagger} = V\sqrt{I - \mathcal{H}^2}, \\ \mathcal{B} &= \sqrt{\mathcal{B}^\dagger\mathcal{B}} W = \sqrt{I - \mathcal{H}^2} W, \end{aligned} \quad (6)$$

where  $V$  and  $W$  are semi-unitary operators such that  $V^\dagger V = WW^\dagger = I$  on the Hamiltonian register.

In the LCU realization, the phases are fixed so that  $V = W = I$ . Substituting these choices into 6 and 5 followed by applying the controlled Pauli-Z operator to the ancillary register produces the  $R_y$  rotation form. Thus, we can see that  $U$  enacts the  $R_y$  operator in each qubitized subspace [37].

$$U = \begin{pmatrix} \mathcal{H} & -\sqrt{I - \mathcal{H}^2} \\ \sqrt{I - \mathcal{H}^2} & \mathcal{H} \end{pmatrix}. \quad (7)$$

More details on this encoding technique can be found in the Appendix A.

The next task is to obtain a polynomial function of  $\mathcal{H}$  from a polynomial function of  $U$ . This is accomplished by noting that the powers of  $U$  generate Chebyshev polynomials of  $\mathcal{H}$ :

$$U^k = \begin{pmatrix} T_k(\mathcal{H}) & * \\ * & * \end{pmatrix}, \quad (8)$$

where  $T_k(\mathcal{H})$  denotes the  $k$ -th Chebyshev polynomial evaluated at  $\mathcal{H}$ . Consequently, the operator  $P(U)$  constructed via the GQSP block encodes a linear combination of Chebyshev polynomials of  $\mathcal{H}$ , which in turn can represent any polynomial function of  $\mathcal{H}$ .

### B. Quantum power iteration method (QPI)

Power iteration is a well-known technique to find the largest eigenvalue of a matrix  $H$ . The underlying idea

is straightforward: one chooses an initial guess for the eigenvector,  $|\psi^{(0)}\rangle$ , that has a nonzero overlap with the true ground state eigenvector, under the assumption that the ground state eigenvalue  $\lambda_1$  has the largest absolute value among all eigenvalues of  $H$ . The iterative procedure is then defined by

$$|\psi^{(n+1)}\rangle = \frac{H|\psi^{(n)}\rangle}{\|H|\psi^{(n)}\rangle\|}. \quad (9)$$

The convergence rate of this method scales as  $(\lambda_2/\lambda_1)^n$ , where  $\lambda_2$  is the second largest eigenvalue. Consequently, a larger spectral gap between  $\lambda_1$  and  $\lambda_2$  generally improves convergence.

From Eq. (9), it follows that the  $n$ -th iteration can be viewed as applying a polynomial of  $H$  to the initial state:

$$|\psi^{(n)}\rangle = \frac{P(H)|\psi^{(0)}\rangle}{\|P(H)|\psi^{(0)}\rangle\|} = \frac{H^n|\psi^{(0)}\rangle}{\|H^n|\psi^{(0)}\rangle\|}. \quad (10)$$

We can implement this polynomial transformation using the GQSP algorithm. In particular, powers of  $\mathcal{H}$  can be expressed as linear combinations of Chebyshev polynomials. The general formula is the following:

$$\mathcal{H}^n = 2^{1-n} \sum_{\substack{k=0 \\ k \equiv n \pmod{2}}}^n \binom{n}{\frac{n-k}{2}} T_k(\mathcal{H}), \quad (11)$$

where  $\sum'$  means that the coefficient corresponding to  $k = 0$  is halved. In the following sections, we demonstrate a practical implementation of QPI and compare its performance with alternative methods.

The main disadvantage of this power method and all the other methods presented in this paper is that its success probability can be very small. It is equal to the square of the denominator in equation 10. A higher probability of success can be achieved with a better initial guess wave function  $|\psi^{(0)}\rangle$ . However, in general, one would require to use amplitude amplification, which would significantly deepen the circuit.

### C. Quantum power Lanczos method (QPL)

The power Lanczos (PL) method is a modification of the standard power iteration approach, aiming to accelerate convergence by improving the initial guess for the eigenvector using Lanczos polynomials [38]. In essence, the Lanczos algorithm constructs a Krylov subspace and finds an approximate ground state eigenvector by diagonalizing a tridiagonal projection of the original Hamiltonian. By treating this approximate ground state as the initial vector in subsequent power iterations, one can often achieve more rapid convergence than with naive power iteration.

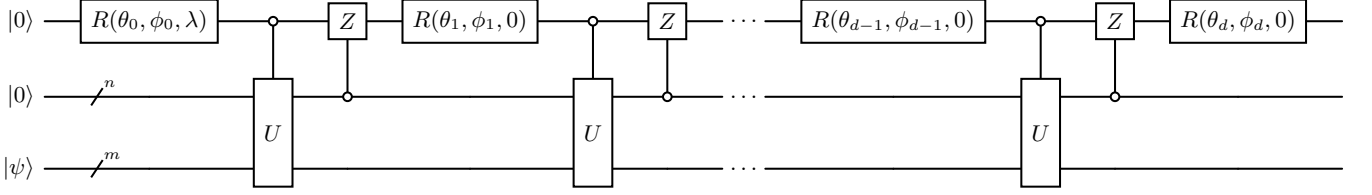


FIG. 1: Generalized Quantum Signal Processing (GQSP) circuit. The circuit comprises three registers: the first one qubit register controls the GQSP procedure, the second  $n$  qubits register performs the block encoding, and the third  $m$  qubits register holds the state on which the Hamiltonian acts.

The classical Lanczos algorithm is a well-known technique for computing several largest in absolute value eigenvalues of a matrix. To accomplish this, one projects the matrix  $H$  onto a Krylov subspace  $\mathcal{K}_d(H, |\psi^{(0)}\rangle)$ , which can be defined as follows:

$$\mathcal{K}_d(H, |\psi^{(0)}\rangle) = \text{span}\{|\psi^{(0)}\rangle, H|\psi^{(0)}\rangle, H^2|\psi^{(0)}\rangle, \dots, H^{d-1}|\psi^{(0)}\rangle\}, \quad (12)$$

where  $d$  is the dimension of the subspace and  $|\psi^{(0)}\rangle$  is the initial state. Numerically stable implementations of the Lanczos algorithm use an orthonormal basis for this subspace. One standard way to build this orthonormal basis is via the recurrence

$$\begin{aligned} |\phi^{(0)}\rangle &= H|\psi^{(0)}\rangle - a_1|\psi^{(0)}\rangle, \\ |\phi^{(n)}\rangle &= H|\psi^{(n)}\rangle - a_n|\psi^{(n)}\rangle - b_n|\phi^{(n-1)}\rangle, \end{aligned} \quad (13)$$

where  $|\phi^{(n)}\rangle$  form a new orthonormal basis,  $a_n = \langle \psi^{(n)} | H | \phi^{(n)} \rangle$  and  $b_n = \sqrt{\langle \phi^{(n-1)} | \phi^{(n-1)} \rangle}$ .

In this basis, the matrix representation of  $H$  becomes tridiagonal, drastically simplifying its partial diagonalization. The eigenvalues and eigenvectors of this tridiagonal subproblem approximate those of the original matrix  $H$ . The approximation can be systematically improved by enlarging the dimension of the Krylov subspace  $d$ , although the rate and quality of convergence also depend on the distribution of eigenvalues and their relative gaps.

Although the standard Lanczos method provides a direct way to compute the tridiagonal representation and its eigendecomposition, it can be advantageous to treat the coefficients in the resulting Krylov vector expansion as variational parameters. In that approach, the energy  $\langle \Psi | H | \Psi \rangle$  is minimized in a trial state  $|\Psi\rangle$  in the Krylov subspace. The main advantage of this approach is that it eliminates the need to precisely calculate the matrix elements of the effective Hamiltonian inside the Krylov space. For the ground state problem, this minimization reproduces the usual Lanczos result, but can offer improved numerical stability.

Consider, for example, a Krylov subspace of dimension  $k+1$ . A generic trial state then has the form

$$\begin{aligned} |\Psi_1^{(0)}\rangle &= |\psi^{(0)}\rangle + C_1 H |\psi^{(0)}\rangle, \\ |\Psi_2^{(0)}\rangle &= |\psi^{(0)}\rangle + C_1 H |\psi^{(0)}\rangle + C_2 H^2 |\psi^{(0)}\rangle, \end{aligned} \quad (14)$$

and so on. The coefficients  $C_i$  may be determined by solving linear equations derived from the tridiagonal matrix or, as advocated here, by performing a variational minimization of the energy. Because  $k$  is often small, this optimization involves only a small number of parameters, therefore it avoids most of the problems related to VQE.

Once the optimized Krylov (Lanczos) state  $|\Psi_k^{(0)}\rangle$  is determined, we use it as a more refined starting point for the power iteration. That is, instead of  $|\psi^{(0)}\rangle$ , we initialize our iterative procedure with  $|\Psi_k^{(0)}\rangle$ . The subsequent  $n$ -th power iteration state can then be written as

$$\begin{aligned} |\Psi_k^{(n)}\rangle &= \frac{1}{N} H^n |\Psi_k^{(0)}\rangle = \\ &= \frac{1}{N} H^n (1 + C_1 H + \dots + C_k H^k) |\psi^{(0)}\rangle, \end{aligned} \quad (15)$$

where  $N$  is a normalization factor and the operator acting on the state(s) can be naturally implemented within the QSP framework. GQSP demonstrates its advantage here over conventional QSP, since during optimization, in order to improve convergence, the parameters  $C_i$  can become complex. Although the coefficients will ultimately be real when calculated without taking the magnetic interaction into account, entering the complex plane in this way allows one to find a workaround to the minimum.

In practice, the QPL method proceeds in two main steps:

1. **Variational Lanczos state preparation.** Build  $|\Psi_k^{(0)}\rangle$  using a polynomial in  $H$  (truncated at order  $k$ ) using GQSP, then optimize the coefficients  $\{C_i\}$  to minimize  $\langle \Psi_k^{(0)} | H | \Psi_k^{(0)} \rangle$ . Although one can solve for  $\{C_i\}$  analytically using the Lanczos tridiagonalization, this requires computing expectation values of multiple powers of  $H$ . In many quantum settings, a small variational optimization with a handful of coefficients is simpler.
2. **Quantum power iteration.** After obtaining  $|\Psi_k^{(0)}\rangle$ , perform the standard power iteration (Eq. (15)) using this improved initial guess.

We show further that even small Krylov subspace ( $k=1$  or  $k=2$ ) often suffice to provide a significantly better initial state. The larger  $k$  yields a more difficult optimization landscape, but often offers insignificant

gains in terms of accuracy. Thus, the QPL method can serve as a middle ground: it leverages a minimal Lanczos subspace to speed up convergence in power iteration introducing only a few parameters.

Overall, this QPL approach can noticeably outperform pure power iteration for ground state computations, particularly when the spectrum of  $H$  has a large gap or when a small Krylov space already captures a significant fraction of the ground state component in  $|\psi^{(0)}\rangle$ .

#### D. Quantum inverse iteration method (QII)

Inverse iteration is another classical technique for iteratively solving eigenvalue problems. Unlike power iteration, which is naturally suited for finding the dominant eigenvalue and its corresponding eigenvector, inverse iteration can be used to approximate any eigenpair, provided that an appropriate shift is chosen. Specifically, one starts with an initial guess for the eigenvector  $|\psi_m^{(0)}\rangle$ , and an approximate eigenvalue  $\epsilon_m$ , close to the true eigenvalue  $\lambda_m$ . The iterative step is given by

$$|\psi_m^{(n+1)}\rangle = \frac{(H - \epsilon_m I)^{-1} |\psi_m^{(n)}\rangle}{\|(H - \epsilon_m I)^{-1} |\psi_m^{(n)}\rangle\|}. \quad (16)$$

Here, the convergence rate depends on how well  $\epsilon_m$  approximates the target eigenvalue  $\lambda_m$ . Quantitatively, if  $\lambda_l$  is the eigenvalue closest to  $\epsilon_m$  other than  $\lambda_m$ , the error term scales as  $\left|(\epsilon_m - \lambda_m)/(\epsilon_m - \lambda_l)\right|^n$ . Hence, choosing  $\epsilon_m$  closer to  $\lambda_m$  accelerates convergence.

By repeated application of  $(H - \epsilon_m I)^{-1}$ , we see that the  $n$ -th iterate can be written as:

$$|\psi_m^{(n)}\rangle = \frac{(H - \epsilon_m I)^{-n} |\psi_m^{(0)}\rangle}{\|(H - \epsilon_m I)^{-n} |\psi_m^{(0)}\rangle\|}. \quad (17)$$

To implement this step through the GQSP framework, we require a polynomial approximation to the operator  $(H - \epsilon_m I)^{-n}$ . The Taylor power series expansion for negative powers of a shifted operator is given by

$$(H - \epsilon_m I)^{-n} = (-1)^n \sum_{k=0}^{\infty} \binom{n+k-1}{k} \frac{1}{(\epsilon_m)^{n+k}} H^k. \quad (18)$$

In principle, one can truncate this infinite series to obtain a polynomial in  $H$ . The radius of convergence for this expansion is  $\|H\| < |\epsilon_m|$ . In practice, this condition can be restrictive for excited state calculations because we want  $\epsilon_m$  to be as close as possible to  $\lambda_m$ . Strictly speaking, we need  $\epsilon_m$  to be outside the spectral radius of  $H$ , that is,  $\|H\| < |\epsilon_m|$ , to guarantee convergence of the series. This is most naturally satisfied if  $\lambda_m$  is the ground-state energy and  $\epsilon_m$  is chosen to be slightly larger than  $\lambda_m$ . In this scenario, one can often achieve more

rapid convergence compared to QPI, thanks to the favorable shift.

Just as in the power iteration method, a key step in QII is to map the truncated power series onto a polynomial expansion in terms of Chebyshev polynomials, which are naturally compatible with QSP. In an actual GQSP implementation, the Hamiltonian  $H$  and the shift  $\epsilon_m$  are further scaled by the  $\ell_1$ -norm of  $H$  to ensure that the argument of the Chebyshev polynomials lies within their domain of convergence. Once the polynomial representation is finalized, the same QSP techniques used for power iteration can be used to apply  $(H - \epsilon_m I)^{-n}$  to a quantum state.

The full power of GQSP becomes apparent when a complex energy shift  $z = \epsilon_m + i\gamma$  is introduced. Although we do not employ it in the examples below, this shift both regularizes the pole at  $E = \epsilon_m$  and enlarges the radius of convergence of the Taylor power series expansion by displacing singularities off the real axis. Concretely, the shifted resolvent  $(H - zI)^{-1}$  remains finite at  $E = \epsilon_m$  and, in the spectral representation, its squared magnitude takes the Lorentzian form  $|(H - zI)^{-1}|^2 = ((H - \epsilon_m I)^2 + \gamma^2 I)^{-1}$ . The width parameter  $\gamma$  governs the trade-off between spectral selectivity (a narrow peak for small  $\gamma$ ) and numerical stability or convergence speed (larger  $\gamma$  produces better conditioning). Finally, note that  $(H - zI)^{-1}$  is precisely the Green's function of  $H$  evaluated at  $z$ , establishing a direct connection to the contour integral and filter diagonalization eigensolvers and other Green's function methods.

#### E. Quantum folded spectrum method (QFSM)

To compute excited states within the GQSP framework, one can employ an iterative version of the folded spectrum method. The key idea is to construct a modified operator

$$H' = I - C(H - \epsilon_m I)^2, \quad (19)$$

where  $\epsilon_m$  is an estimate of the target eigenvalue and  $C$  is an appropriately chosen constant. Upon focusing on  $(H - \epsilon_m I)^2$ , one effectively "folds" the spectrum around  $\epsilon_m$ . After scaling with  $C$  and shifting by identity, the eigenvalue closest to  $\epsilon_m$  in the original spectrum becomes the largest eigenvalue of  $H'$ , so it can be achieved via a power iteration scheme:

$$|\psi_m^{(n+1)}\rangle = \frac{(I - C(H - \epsilon_m I)^2) |\psi_m^{(n)}\rangle}{\|(I - C(H - \epsilon_m I)^2) |\psi_m^{(n)}\rangle\|}. \quad (20)$$

Repeating this step  $n$  times yields

$$|\psi_m^{(n)}\rangle = \frac{(I - C(H - \epsilon_m I)^2)^n |\psi_m^{(0)}\rangle}{\|(I - C(H - \epsilon_m I)^2)^n |\psi_m^{(0)}\rangle\|}. \quad (21)$$



Since  $(I - C(H - \epsilon_m I)^2)^n$  is a polynomial in  $H$ , it is naturally suited to GQSP implementations. In practice, the Hamiltonian is first shifted by replacing  $H$  with  $H_{\text{shifted}} = H - \epsilon_m I$ . Specifically, shifting only alters the identity term in the LCU construction. After this shift, the polynomial

$$(1 - CH_{\text{shifted}}^2)^n = \sum_{k=0}^n \binom{n}{k} \frac{1}{(-C)^k} H_{\text{shifted}}^{2k} \quad (22)$$

can be applied exactly to the quantum state. However, convergence in this folded spectrum scheme depends sensitively on the choice of  $\epsilon_m$ , the initial guess  $|\psi_m^{(0)}\rangle$ , and the constant  $C$ . In typical implementations,  $C$  is chosen so that the shifted square spectrum lies between 0 and 1, which facilitates faster convergence. However, the initial state can have an even more profound effect on performance, as will be illustrated in the next section.

Table I summarizes the polynomial forms of all the methods discussed in this work.

TABLE I: Summary of the polynomial expansions that underlie each quantum iterative method (QPI, QPL, QII, and QFSM). Here,  $\epsilon_m$  is the target eigenvalue approximation, and  $C$  is chosen to ensure the folded-spectrum operator is suitably bounded.

Method	Polynomial Form
QPI	$H^n$
QPL	$H^n \sum_{i=0}^N c_i H^i$
QII	$(-1)^n \sum_{k=0}^{\infty} \binom{n+k-1}{k} \frac{1}{(\epsilon_m)^{n+k}} H^k$
QFSM	$\sum_{k=0}^n \binom{n}{k} \frac{1}{(-C)^k} H_{\text{shifted}}^{2k}$ , where $H_{\text{shifted}} = H - \epsilon_m I$

### III. COMPUTATIONAL DETAILS

We provide here the computational setup for the proof-of-concept numerical simulations of our proposed methods. Reference CASCI calculations were performed using the PySCF package [39]. The Jordan–Wigner transformed molecular Hamiltonians used in our simulations were generated with the QuKet package [40].

Except for QFSM, all simulations employed the qubit tapering technique to reduce the number of qubits [41, 42]. For example, the  $H_2$  molecule in a (2, 2) active space required only 1 qubit instead of 4;  $CH_2$  in a (6, 6) active space required 8 qubits instead of 12; and  $N_2$  in a (6, 6) space required 7 qubits instead of 12.

The GQSP circuit shown in Fig. 1 was implemented using the Qulacs simulator [43]. Angle estimation was

performed using Prony’s method [44], described in detail in the Appendix B. The *capitalization* step required one additional qubit.

Block encoding was implemented using the LCU method only for the  $H_2$  system, which required two additional qubits. For other systems, to maintain computational feasibility, we employed an explicit block encoding scheme using a single additional qubit, as illustrated in Eq. 7. Although in practical implementation on a quantum device the LCU is necessary, we used this trick for performance verification purposes. More details are provided in Appendix B. The complete implementation is available on our GitHub repository: <https://github.com/mizukami-group/power-lanczos-data-FY2025.git>.

## IV. RESULTS AND DISCUSSION

### A. Comparison of QPI and QPL

We first performed numerical tests of the QPI and QPL methods. Since QPL can be viewed as a direct modification of QPI, we discuss both in this section. Following the notation introduced in Eq. 15, we denote by QPL $k$  the QPL method of the Lanczos polynomial degree  $k$ . In this notation, the QPI method corresponds to QPL0.

Figure 2 shows the potential energy curves (PECs) for the hydrogen molecule using the cc-pVDZ basis set with 2 electrons in 2 active orbitals. The Hartree-Fock (HF) wave function served as the initial guess.

We observe that the QPI (QPL0) method achieves the CASCI(2, 2) energy to within chemical accuracy in no more than 6 iterations, even when starting from the HF wave function. For longer bond lengths, more iterations are required to reach chemical accuracy, reflecting the increased multireference character of the wavefunction. This behavior becomes more pronounced as the bond is stretched, indicating that the method may converge more slowly for systems with stronger static correlation.

We also note that the convergence speed of a power method depends on the ratio  $E_2/E_1$ , where  $E_1$  and  $E_2$  denote the ground state and first excited state energies, respectively. Indeed, the right panels of Fig. 2 show that the convergence rates are roughly proportional to  $\log_{10}(E_2/E_1)$ , with a proportionality coefficient between 1.85 and 2 at different bond lengths.

Next, we examine QPL1, where the final wave function after optimizing the Lanczos polynomial at degree 1 reads

$$|\text{QPL1}\rangle = \frac{1}{N} (a_0 + a_1 H) |\text{HF}\rangle. \quad (23)$$

and  $N$  is the normalization factor. Remarkably, this ansatz can match the CASCI energy immediately after the polynomial optimization, before any additional power method steps.

Figure 3 illustrates how the Lanczos polynomial coefficients  $a_0$  and  $a_1$  vary with the bond length. We observe

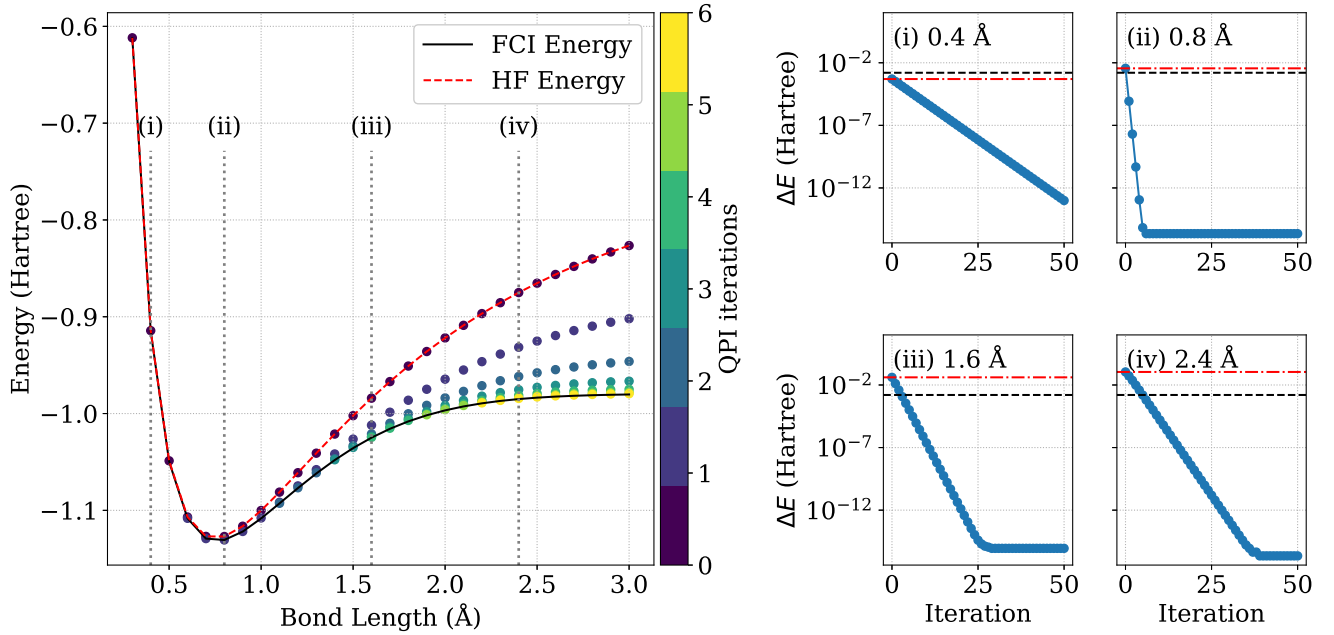


FIG. 2: Potential energy curve for the hydrogen molecule obtained with the QPI method (i.e., QPL0). The basis set is cc-pVDZ and the active space is (2, 2). The left panels show the energy deviation from CASCI(2, 2) at each iteration for the first 50 iterations. The coefficient  $k$  is the slope of the linear portion of the convergence plot. The black dashed line indicates chemical accuracy (1 kcal/mol), and the red dot-dashed line is the HF energy.

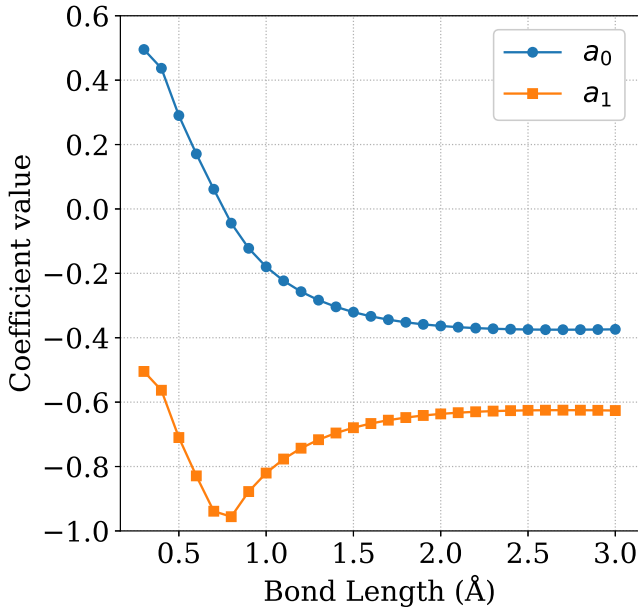


FIG. 3: Bond length dependence of the Lanczos polynomial coefficients for the hydrogen molecule.

that  $a_0$  changes sign around the equilibrium geometry of  $H_2$ . Since  $a_0$  represents the HF component of the wave function, its sign change reflects the decreasing HF contribution as the bond stretches. Meanwhile,  $a_1$ , which

weighs  $H|HF\rangle$ , reaches its maximum near the equilibrium geometry and then decreases. This behavior is expected because  $H|HF\rangle$  is not orthogonal to  $|HF\rangle$ , so the relative amplitudes of these two contributions can offset each other.

Next, we computed the PECs of the singlet and triplet states of the  $CH_2$  radical. The cc-pVDZ basis set with 6 electrons in 6 active orbitals was employed, and both C–H bonds were stretched symmetrically while keeping the H–C–H angle fixed at  $101.89^\circ$ . For the singlet state, we used the restricted Hartree-Fock (RHF) wave function as an initial guess; for the triplet state, we used the restricted open-shell Hartree-Fock (ROHF) wave function. The results are shown in Fig. 4.

It is well known that the triplet state lies below the singlet state around the equilibrium geometry of  $CH_2$ . For both spin states, QPL $k$  yields a marked improvement over the respective HF initial guesses. However, in contrast to the hydrogen molecule, QPL0 (QPI) fails to achieve chemical accuracy after 50 iterations for bond lengths beyond roughly 1.5 Å in the triplet and for all bond lengths in the singlet. Hence, to reach chemical accuracy, we need to optimize Lanczos polynomials to a higher degree. As the bond stretches, this need becomes more pronounced, consistent with the growing multireference character of the wave function.

In addition, there are insignificant gains from higher-degree polynomials, and, in practice, convergence of the polynomial coefficients can become more challenging at

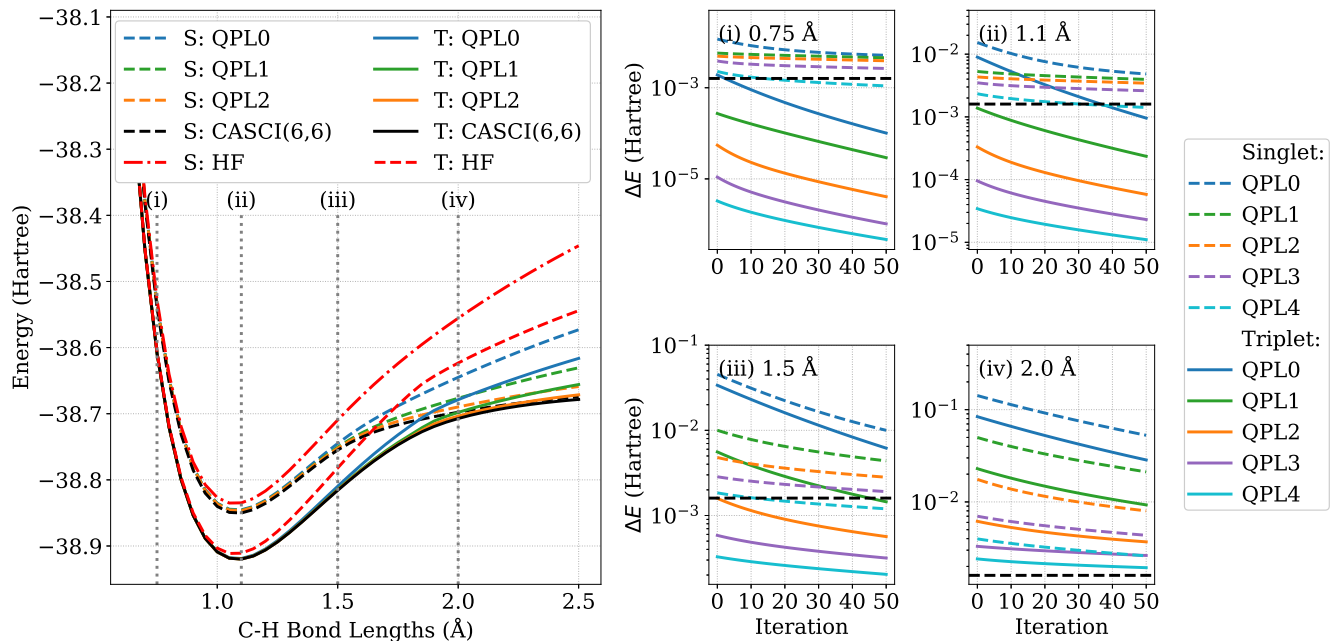


FIG. 4: Potential energy curves for singlet (S) and triplet (T)  $\text{CH}_2$  obtained using QPL. The basis set is cc-pVDZ with an active space of (6,6). The left panel shows the PECs at various polynomial degrees ( $k = 0, 1, 2$ ). The right panels show deviations from CASCI(6,6) for the first 50 iterations of the power method using QPL with  $k = 0, 1, 2, 3, 4$ . The dashed black lines indicate chemical accuracy (1 kcal/mol). Solid lines correspond to the triplet state and dashed lines to the singlet state.

large  $k$ . Thus, it is generally advisable to use moderate polynomial degrees (up to  $k = 2$ ). This observation aligns with Ref.[38]. However, there are exceptions, as with the 0.75 Å bond length in Fig. 4, where QPL4 converges unusually fast. In such cases, an important configuration may be connected to the reference state only through a series of four excitations.

Finally, we note that the singlet state, with its lower spin, displays a stronger multireference character than the triplet state, generally requiring higher degree Lanczos polynomials to achieve comparable accuracy.

As a further test, we applied QPL to the nitrogen molecule, which is well known to have a highly multireference character of the ground state in stretched geometries. We used the cc-pVDZ basis set with 6 electrons in 6 active orbitals. Two different initial guesses were tested:

1. The RHF wave function.
2. A partially converged VQE wave function with a UCCD ansatz (after only 2 iterations), which is thus multireference but not fully optimized.

The corresponding PECs are presented in Fig. 5.

For equilibrium geometry, QPL0 cannot match the CASCI(6,6) energy within 50 iterations, but QPL1 succeeds. However, at longer bond lengths (1.5 Å and 2.0 Å), even QPL3 does not achieve chemical accuracy. These results reiterate that highly multireference systems

pose convergence challenges for QPI and QPL, although higher-degree polynomials often help.

A more effective approach is to use a better initial guess than HF. Indeed, starting from the partially converged UCCD wave function significantly improves the convergence, allowing us to achieve chemical accuracy at longer bond lengths. However, for stretched geometries (e.g., 2.0 Å in Fig. 5), even this better initial guess is insufficient without further refinements.

Overall, these results demonstrate that QPI and QPL are far more effective in refining a reasonably good reference wave function, one that captures most of the static correlation, rather than attempting to recover both static and dynamic correlation from a simple HF state. This use case was precisely the motivation for the original power Lanczos approach in Ref. [38], where the method was used to add dynamic correlation to Monte Carlo wave functions already containing strong static correlation.

## B. Numerical Results for QII

In this section, we demonstrate the performance of the GQSP-based QII algorithm. We first present a PEC calculation as an illustrative example. We then compare our implementation of QII with two existing methods, I-Iter and Q-Inv, which rely on linear combinations of imaginary-time evolution operators [27].



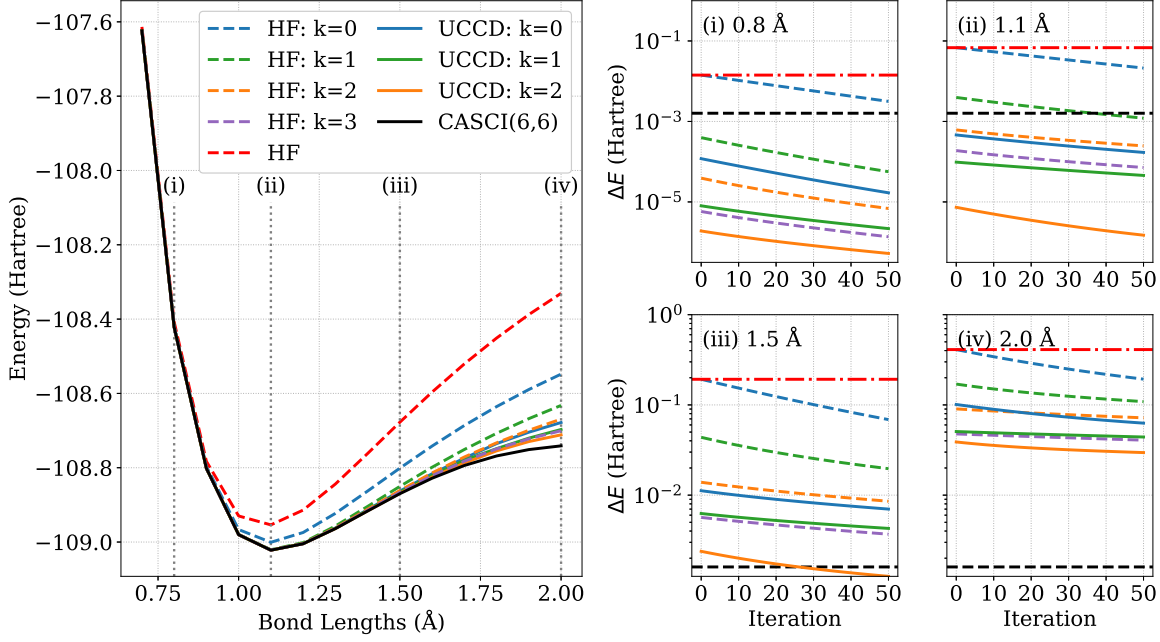


FIG. 5: Potential energy curves for the nitrogen molecule obtained using QPL. The basis set is cc-pVDZ and the active space is (6,6). The left panel shows PECs from QPL with different polynomial degrees ( $k = 0, 1, 2, 3$ ) and initial guesses (HF in dashed, and partially converged UCCD in solid). The right panels display energy differences from CASCI(6,6) over the first 50 iterations of the power method. The black dashed line marks chemical accuracy (1 kcal/mol), and the red dot-dashed line is the HF energy.

We begin by examining the dissociation curve of the hydrogen molecule. Calculations use the cc-pVDZ basis set with 2 electrons in 2 active orbitals. In QII, the inverse operator is approximated by truncating the Taylor polynomial to some degree  $n$ . We present results for  $n = 2, 5$ , and 10. QII also requires an initial estimate of the ground state energy, which we take as the HF energy. Figure 6 displays the resulting PECs.

We observe that the ability to reach the CASCI(2,2) energy within chemical accuracy depends on the degree  $n$  of the truncated polynomial. For example, at a bond length of 1.6 Å, QII( $n = 2$ ) converges to a value above chemical accuracy and similarly, QII( $n = 5$ ) struggles at 2.4 Å. In contrast, for sufficiently large  $n$  ( $n = 50$ ), the method achieves chemical accuracy in only one iteration for all bond lengths. This rapid convergence outperforms the QPI method, reflecting the fact that the ground state wave function becomes increasingly multireference at longer bond lengths and thus benefits substantially from the inverse operator approach.

Next, we compare our GQSP implementation of QII with the I-Iter and Q-Inv algorithms, which evaluate  $H^{-1}$  or  $H^{-k}$  by numerically integrating imaginary-time evolution operators [27]. The I-Iter method approximates  $H^{-1}$  via

$$H^{-1} = \frac{i}{\sqrt{2\pi}} \int_0^\infty dy \int_{-\infty}^\infty dz z e^{-z^2/2} e^{-iyzH}. \quad (24)$$

and repeated application of  $H^{-1}$  ( $k$  times) gives  $H^{-k}$ . The Q-Inv method, proposed by Kyriienko [26], directly approximates  $H^{-k}$  by

$$H^{-k} = \frac{iN_k}{\sqrt{2\pi}} \int_0^\infty dy \int_{-\infty}^\infty dz z y^{k-1} e^{-z^2/2} e^{-iyzH}, \quad (25)$$

where  $N_k$  is a normalization constant. Both I-Iter and Q-Inv use the Gauss-Legendre rule to calculate the integrals, and the precision of this procedure depends on the order of the Legendre polynomials used. In Ref. [27], comparisons are made for two orders  $n_y$  for integration of the variable  $y$ , in particular  $n_y = 1$  and  $n_y = n_{\text{eq}}$ , where  $n_{\text{eq}}$  is the order sufficient to achieve energy convergence.

Analogously to the reference paper, we investigate four molecules:  $\text{H}_2$ , LiH,  $\text{BeH}_2$ , and a square  $\text{H}_4$ , using a STO-6G basis set. For  $\text{H}_2$  and  $\text{H}_4$  full active spaces were used, (2,2) and (4,4) respectively. For LiH 2 electrons in 5 orbitals and for  $\text{BeH}_2$  4 electrons in 5 orbitals were used. All calculations are single-point, with geometries of 0.75 Å for  $\text{H}_2$ , 1.23 Å for the H-H distance in  $\text{H}_4$ , 1.6 Å for the Li-H bond in LiH, and 1.326 Å for the Be-H bond in  $\text{BeH}_2$ . In this section and in figure 7 we compare only QII with truncation  $n = 50$  with Q-Inv and I-Iter with  $n_y = n_{\text{eq}}$ . The results for different truncations are discussed in the Appendix C. During a comparison of the number of qubits between the methods, we assumed the LCU block encoding. We also included qubit counts with the use of qubit tapering.

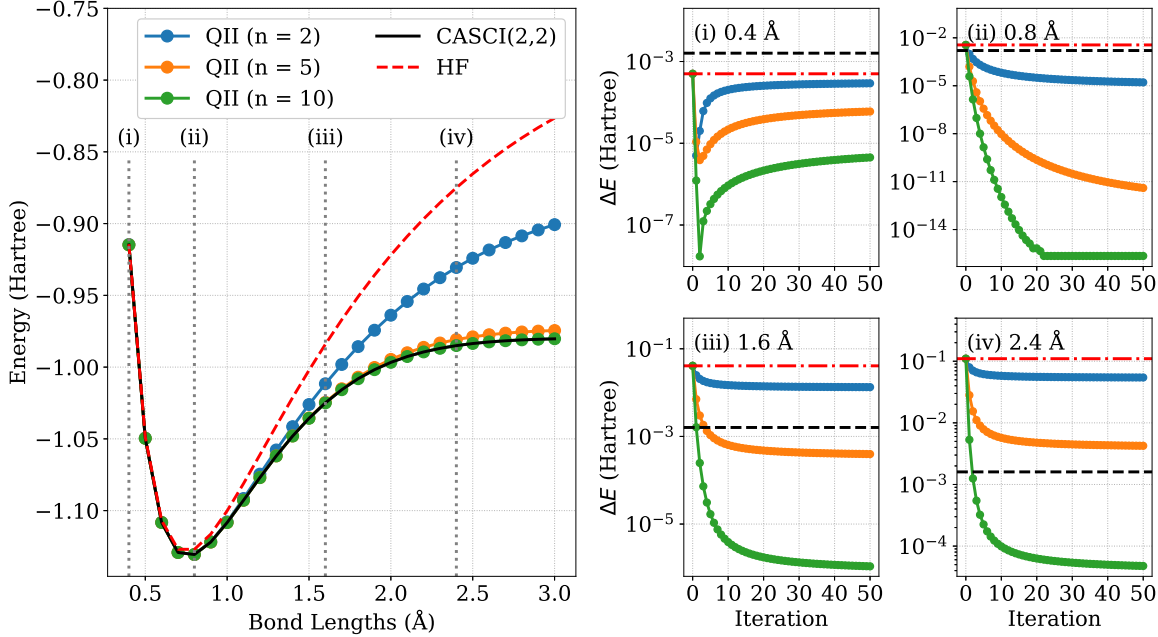


FIG. 6: Potential energy curves for the hydrogen molecule obtained using QII with different polynomial truncation degrees ( $n = 2, 5, 10$ ). The basis set is cc-pVDZ and the active space is (2, 2). The right panels show the deviation from the CASCI(2, 2) energy over the first 50 iterations. The black dashed lines mark chemical accuracy (1 kcal/mol), and the red dot-dashed lines represent the HF energy.

For the simplest system  $H_2$  chemical accuracy was achieved quickly with all methods. QII and Q-Inv+I-Iter were able to achieve machine precision. Q-Inv started to diverge after 3 iterations. Let us estimate the resources needed for these calculations. For QII the number of qubits is constant for all iterations here and equal to 7 (with qubit tapering 4). The number of qubits for Q-Inv and I-Iter is equal to at least 13. However, since we used truncation degree 50, we needed the same number of queries to the block encoded Hamiltonian, which makes the circuit deep. Q-Inv and I-Iter do not require queries to block encoding, but on the other hand require Trotter approximation of time-evolution operator, which also can be relatively deep.

For LiH all methods were also eventually able to achieve chemical accuracy. However, QII did it in 3 iterations, while Q-Inv and I-Iter required more than 10. Q-Inv also started to severely diverge after 14 iterations. This divergent behavior was fixed in the combined implementation of Q-Inv and I-Iter. For QII the number of qubits is equal to 11 (with qubit tapering 7). The number of qubits for Q-Inv and I-Iter is equal to at least 17. We used the same truncation degree 50, therefore, we needed the same number of queries to the block encoded Hamiltonian.

In case of  $BeH_2$  QII achieved chemical accuracy in one iteration, while Q-Inv and I-Iter required more than 10. Generally, Q-Inv and I-Iter demonstrate a behavior similar to that of LiH. The resources requirement is also the

same as for LiH. QII needs 11 qubits (with qubit tapering 7), whereas Q-Inv and I-Iter require at least 17. The number of queries to block encoding is the same as before.

The last system tested was square  $H_4$ . It was a difficult case for Q-Inv, which converged before reaching chemical accuracy. QII and I-Iter were more successful. Although QII with  $n = 50$  demonstrates a very fast reach to the chemical accuracy, with smaller truncation it has the problem of early convergence, analogously to Q-Inv (see Appendix C). QII needs 9 qubits (with qubit tapering 7), whereas Q-Inv and I-Iter require at least 15.

In summary, our GQSP-based QII implementation offers several advantages. First, implementing the time-evolution operator in I-Iter and Q-Inv typically involves Suzuki-Trotter decompositions, which introduce additional errors and increase the circuit depth. Second, I-Iter and Q-Inv require LCU approaches to approximate the integral, necessitating  $O(\log(n_y n_z))$  auxiliary qubits, where  $n_y$  and  $n_z$  correspond to orders of Legendre polynomials in numerical integration of Eq. 24 and Eq. 25. The authors noted that  $n_z$  depends on the power of the inverse Hamiltonian  $k$ . Moreover, it is not explicitly explained how to apply  $H^{-1}$   $k$  times, using I-Iter. It may require to do state tomography after each step or the use of QSP. The same problem applies to Q-Inv+I-Iter. In contrast, GQSP constantly needs only one signal processing qubit, one qubit for capitalization (if needed), and additionally  $O(\log N)$  qubits for the LCU block encoding, where  $N$  is the number of Pauli terms in the

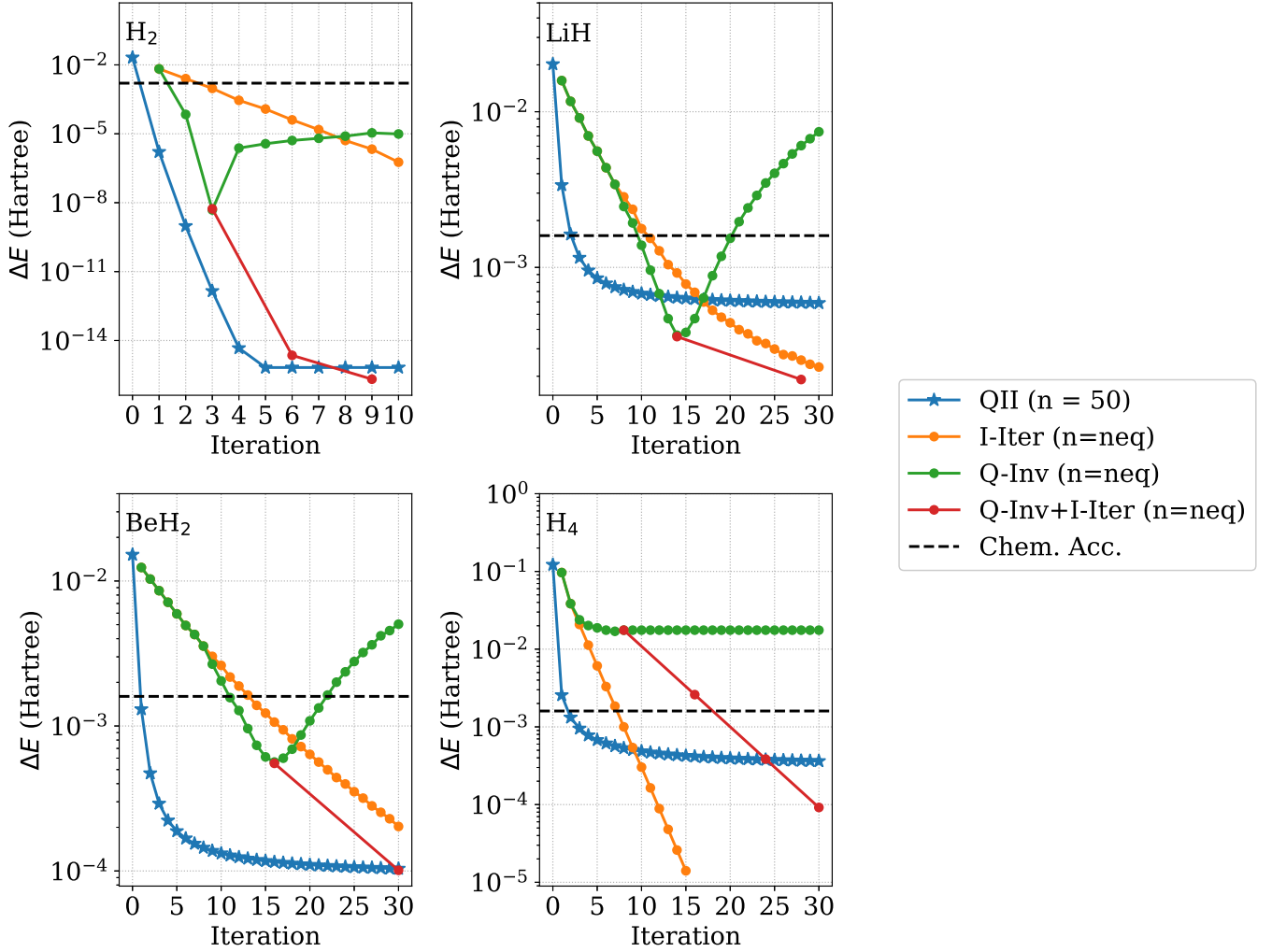


FIG. 7: Comparison of QII, I-Iter, and Q-Inv [27] for  $\text{H}_2$ ,  $\text{LiH}$ ,  $\text{BeH}_2$ , and  $\text{H}_4$ . The deviation from CASCI energies as a function of the iteration number is shown. For QII,  $n = 50$  refers to the Taylor polynomial truncation degree, while for I-Iter and Q-Inv,  $n_y$  is the Gauss-Legendre polynomial order.  $n_{\text{eq}}$  is the order at which energy convergence is reached.

LCU expansion (see A1). In the worst case  $N$  scales as  $O(n_{\text{orb}}^4)$ , leading to  $O(\log n_{\text{orb}})$  ancilla qubits, where  $n_{\text{orb}}$  is the number of orbitals in active space. Third, QII reaches chemical accuracy very fast, having provided a sufficiently large truncation value. However, QII does require a good initial estimate of the ground state energy, which I-Iter and Q-Inv do not. Nevertheless, if such an estimate is available, QII can converge to high accuracy in very few iterations, especially for larger polynomial degrees.

### C. Excited states calculations using QFSM

Finally, we performed numerical tests of the Quantum Folded Spectrum Method (QFSM) implemented using GQSP. Unlike the other algorithms discussed in this

work, QFSM enables access to excited states.

As a first test, we computed the PECs of the ground and excited states in the hydrogen molecule using the cc-pVDZ basis set with an active space of 2 electrons in 2 orbitals. The convergence of QFSM depends critically on the choice of the initial guess wave function, which should have a large overlap with the target excited state. For example, starting from an RHF wave function does not allow convergence to the  $1^3\Sigma_u^+$  triplet state or the  $1^1\Sigma_u^+$  singlet excited state.

To ensure sufficient overlap with specific target states, we employed the following initial guess states:

$$\begin{aligned} |\Psi_{\Sigma_g}\rangle &= |0011\rangle, \\ |\Psi_{\Sigma_u}\rangle &= |1001\rangle, \end{aligned} \quad (26)$$

where the ordering corresponds to  $|\sigma_\beta^* \sigma_\alpha^* \sigma_\beta \sigma_\alpha\rangle$ . As an energy shift in the folded Hamiltonian, we used the corre-

sponding CASCI(2,2) energies for testing purposes. The results are presented in Fig. 8.

The singlet states  $X^1\Sigma_g^+$  and  $2^1\Sigma_g^+$  converged to chemical accuracy across all bond lengths when starting from  $|\Psi_{\Sigma_g}\rangle$ . However, at 0.4 Å and 0.8 Å, a divergence was observed after 25 iterations due to the loss of orthogonality in floating point arithmetic. This is a typical drawback of power iteration methods. The convergence to the  $1^1\Sigma_u^+$  and  $1^3\Sigma_u^+$  states was more challenging when starting from  $|\Psi_{\Sigma_u}\rangle$ . At short bond lengths (0.4 Å and 0.8 Å), these states were unable to reach chemical accuracy, and their convergence was very slow. The right-hand plots show overlapping data points for these two states, indicating near-degeneracy. This behavior can be attributed to the presence of quasi-degenerate eigenstates in the folded Hamiltonian, which causes the wave function to be simultaneously attracted toward both, hindering convergence. Improved initial guesses could resolve this issue.

We also computed PECs for four low-lying electronic states of ethylene along the internal rotation around the double bond. The cc-pVDZ basis set was used, with 2 electrons in 2 active  $\pi$  orbitals. As in the hydrogen case, the convergence strongly depends on the initial guess. The following guess states were used:

$$\begin{aligned} |\Psi_{A_g}\rangle &= |0011\rangle, \\ |\Psi_{B_{1u}}\rangle &= |1001\rangle, \end{aligned} \quad (27)$$

where the orbital ordering is  $|\pi_\beta^*\pi_\alpha^*\pi_\beta\pi_\alpha\rangle$ . As before, CASCI(2,2) energies were used as energy shifts. The results are shown in Fig. 9.

At 0°, all states except the triplet  $^3B_{1u}$  reached chemical accuracy within 50 iterations. The triplet state would likely converge with additional iterations. Convergence was fastest for the singlet  $^1A_g$  states. At 90°, none of the states reached chemical accuracy within the 50 iterations, although convergence trends were still visible. Up to 60°, both singlet  $^1A_g$  states achieved chemical accuracy.

A key advantage of our GQSP-based QFSM implementation over variational quantum eigensolver VQE-based folded spectrum approaches is that we do not need to construct or measure the squared Hamiltonian explicitly. For example, Ref. [45] shows that even for  $H_2$  in the STO-3G basis, constructing the squared Hamiltonian requires measurement of 24 Pauli strings, and for  $H_2O$ , over 111,000 Pauli strings are required. In contrast, our approach does not require additional Pauli measurements and completely avoids variational optimization. The main limitation of our method is that convergence is generally slower and is highly dependent on the quality of both the initial guess wave function and the target energy. Despite this, QFSM is a promising tool for accessing excited states, especially when a good initial state is available.

## V. CONCLUSION

In this work, we demonstrate how GQSP can serve as a unifying framework to implement quantum analogues of power methods, which are useful for initial state preparation. In particular, we introduced and numerically tested the QPI, QPL, and QII methods for ground state calculations, as well as the QFSM for calculating excited states. Our results show that these methods, widely employed in classical linear algebra, can be naturally adapted to quantum hardware via GQSP.

A key feature of the GQSP approach is its resource efficiency. GQSP is efficient in the number of queries to the encoded unitary operator. This is equal to the polynomial degree used in each presented method. Moreover, this approach numerically requires less qubits than existing methods based on a linear combination of time-evolution operators and makes resource estimation predictable and universal for all used methods. Additionally, our approach is free of Trotter decomposition, and therefore has no corresponding errors.

We presented proof-of-concept calculations for several molecular systems to verify the convergence behavior. In particular, we showed that QPL often converges faster and more reliably than QPI, requiring lower polynomial degrees to achieve the same accuracy. In addition, the GQSP-based implementation of QII can outperform existing I-Iter and Q-Inv methods in terms of both the convergence speed and the qubit requirements. QFSM enables excited-state calculations without the need for variational minimization or explicit construction of the squared Hamiltonian, although careful choices of initial states remain important for effective convergence. Note that our implemented methods are equivalent to its classical counterparts and can be run with classical computer if exponential memory is available. To our knowledge, however, there have been no previous cases where power methods using polynomial series expansion were applied to quantum many-body problems for comparative study.

The main disadvantage of our methods is the generally low success probability. It is a typical problem for state preparation techniques using non-unitary transformations, such as imaginary-time evolutions. In practical application, it is required to use either a post-selection with a large number of repetitions, or amplitude amplification. The latter results in an increase of the depth of the circuit several times. Nevertheless, we expect that the problem is less harsh for our power methods than that for imaginary-time evolution.

This research presents a general framework for quantum power methods and its proof of concept; still, considerable work remains before practical implementation. First of all, more accurate resource estimation including amplitude amplification is needed. Also, eliminating the need for variational optimization in QPL by deriving polynomial coefficients from perturbation theory could improve efficiency. The QII method could benefit from replacing the current polynomial approximation of the in-

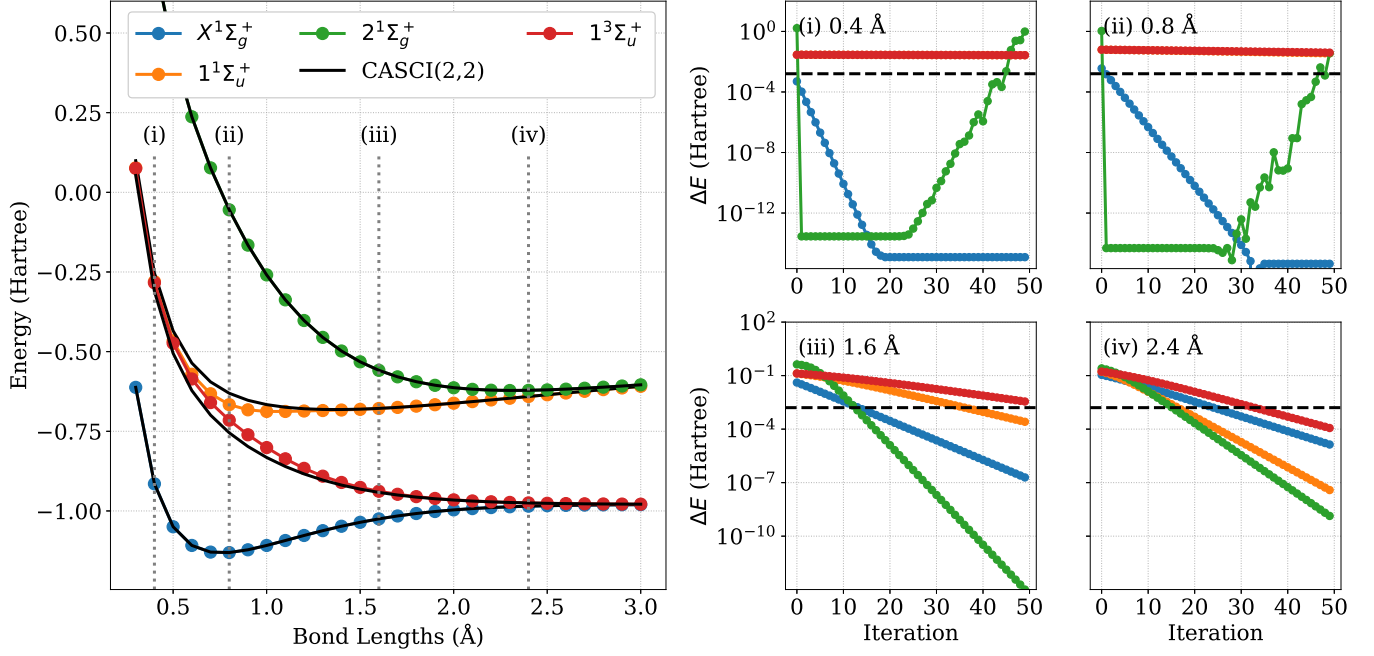


FIG. 8: Potential energy curves for the hydrogen molecule computed using QFSM. The basis set is cc-pVDZ and the active space is (2, 2). The right plots show the energy deviation from CASCI(2, 2) over the first 50 iterations. The black dashed line denotes chemical accuracy (1 kcal/mol).

verse function with one that has a larger radius of convergence, potentially enabling the accurate computation of excited states. In addition, using imaginary energy shifts can be beneficial, and, more generally, Green's function methods can be implemented using this technique. In the case of QFSM, it would be advantageous to identify a function that better distinguishes energy levels, since it is currently common for multiple eigenvalues in the folded spectrum to cluster near 1, greatly worsening convergence. Finally, integration of GQSP-based methods with other quantum-classical hybrid approaches may open the door to tackling larger and more complex molecular systems on near-term quantum devices.

## ACKNOWLEDGMENTS

This work was supported by MEXT Quantum Leap Flagship Program (MEXTQLEAP) Grant No. JPMXS0120319794, the JST COL-NEXT Program Grant No. JPMJPF2014 and JST ASPIRE Program JPMJAP2319. This research was partially facilitated by the JSPS Grants-in-Aid for Scientific Research (KAKENHI) Grant No. JP23H03819. N.Y. is supported by JST Grant Number JPMJPF2221, JST CREST Grant Number JPMJCR23I4, IBM Quantum, JST ASPIRE Grant Number JPMJAP2316, JST ERATO Grant Number JPMJER2302, and Institute of AI and Beyond of the University of Tokyo.

## Appendix A: LCU block encoding

The GQSP algorithm requires the signal operator to be a controlled unitary. Hence, before applying GQSP to a Hamiltonian  $H$ , we must embed  $H$  into a larger unitary operator. A commonly used method to achieve this is the linear combination of unitaries (LCU) approach [46]. The first step is to write the Hamiltonian as a linear combination of Pauli strings, for example, by applying the Jordan–Wigner transformation to a second-quantized Hamiltonian:

$$H_{JW} = \sum_{j=0}^N c_j P_j, \quad (\text{A1})$$

where each  $P_j$  is a tensor product of Pauli matrices, a "Pauli string", and  $c_j$  are the corresponding coefficients.

The construction of LCU block encoding requires an auxiliary register of  $\lceil \log_2(N) \rceil$  qubits to encode coefficients  $c_j$ . Two key gate sequences are introduced:

- **PREPARE**, which acts on the auxiliary register to create a superposition of  $|j\rangle$  states weighted by  $\sqrt{\frac{|c_j|}{\lambda}}$ ,
- **SELECT**, which uses the  $|j\rangle$  state of the auxiliary register to apply the corresponding Pauli operator  $P_j$  with its phase on the main register.



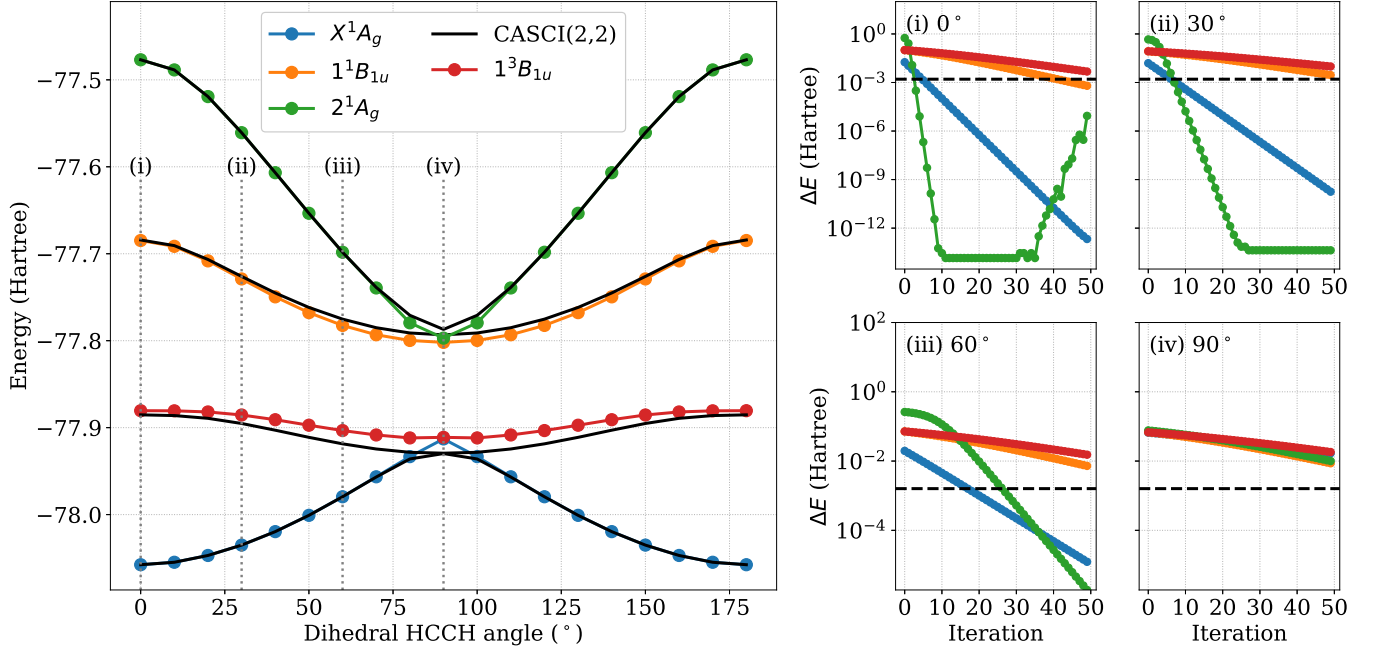


FIG. 9: Potential energy curves for ethylene along the torsional rotation of the double bond, computed using QFSM. The basis set is cc-pVDZ and the active space is (2, 2). The left plots show energy deviation from CASCI(2, 2) over the first 50 iterations. The black dashed line indicates chemical accuracy (1 kcal/mol).

Concretely,

$$\text{PREPARE}|0\rangle = \sum_j \sqrt{\frac{|c_j|}{\lambda}} |j\rangle, \quad (\text{A2})$$

where  $\lambda = \sum_j |c_j|$  is a normalization factor. and

$$\text{SELECT} = \sum_j |j\rangle\langle j| \otimes P_j. \quad (\text{A3})$$

The full LCU operator is implemented as the sequence  $\text{PREPARE}^\dagger - \text{SELECT} - \text{PREPARE}$ , as illustrated in Fig. 10.

Based on paper [37], we can see how the LCU operator acts on the Hamiltonian eigenvectors  $|E_i\rangle$ . For each  $|0\rangle|E_i\rangle$  state there exists an orthogonal state  $|g_i\rangle$ , such that:

$$\begin{aligned} U_{\text{LCU}}|0\rangle|E_i\rangle &= \frac{E_i}{\lambda}|0\rangle|E_i\rangle + \sqrt{1 - \left(\frac{E_i}{\lambda}\right)^2} |g_i\rangle, \\ U_{\text{LCU}}|g_i\rangle &= \sqrt{1 - \left(\frac{E_i}{\lambda}\right)^2} |0\rangle|E_i\rangle - \frac{E_i}{\lambda} |g_i\rangle. \end{aligned} \quad (\text{A4})$$

This shows that  $U_{\text{LCU}}$  acts as a reflection in the two-dimensional invariant subspace spanned by  $\{|0\rangle|E_i\rangle, |g_i\rangle\}_i$ , with matrix:

$$U_{\text{LCU}} = \begin{pmatrix} \mathcal{H} & \sqrt{I - \mathcal{H}^2} \\ \sqrt{I - \mathcal{H}^2} & -\mathcal{H} \end{pmatrix}. \quad (\text{A5})$$

For the purposes of QSP and GQSP, it is often more convenient to work with a rotation matrix rather than a reflection. This is achieved by conjugating  $U_{\text{LCU}}$  with a Pauli-Z gate on the ancilla register. Operationally, this acts trivially if the register is in  $|0\rangle$  and flips the sign if the register is in any other state:

$$U := (Z \otimes I) U_{\text{LCU}} = \begin{pmatrix} \mathcal{H} & -\sqrt{I - \mathcal{H}^2} \\ \sqrt{I - \mathcal{H}^2} & \mathcal{H} \end{pmatrix}. \quad (\text{A6})$$

This operator now acts as an  $\text{SU}(2)$  rotation in each subspace, as required for Chebyshev-based polynomial transformations.

## Appendix B: Angle finding

A crucial component in any QSP-based algorithm is the determination of the rotation angles sequence. The GQSP algorithm is no exception; it uses a procedure very similar to those of conventional QSP and QSVT. The angle finding protocol typically involves four key steps: *truncation*, *partition*, *completion*, and *carving*. We describe each step in detail below.

In GQSP, our goal is to apply an arbitrary function  $f(z)$  to a unitary block encoding matrix  $U$ . As a first step, we approximate the target function by a complex-valued polynomial  $F(z)$ , for example, using the Remez exchange algorithm. This procedure is called *truncation*: restricting the function to a finite-degree polynomial that approximates  $f(z)$  well enough for our purposes.

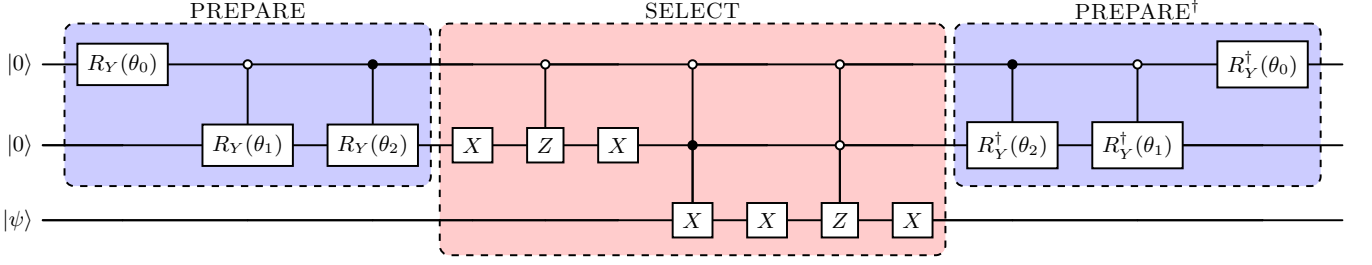


FIG. 10: Quantum circuit for an LCU block encoding of  $H = -aI + bX - cZ$ . The dashed boxes indicate PREPARE (blue) and SELECT (red).

Once we have  $F(z)$ , the next step is partition, in which we rescale  $F(z)$  to ensure that its absolute value does not exceed 1 on the unit circle in the complex plane. Typically, we achieve this by dividing  $F(z)$  by a sufficiently large constant  $\alpha$ , defining  $P(z) = F(z)/\alpha$ . This makes  $|P(z)| \leq 1$  on the complex unit circle.

Having obtained  $P(z)$ , we must then complete the polynomial to form the unitary that GQSP applies to  $U$ . Concretely, we seek a polynomial  $Q(z)$  such that

$$GQSP(U) = \begin{pmatrix} P(U) & \cdot \\ Q(U) & \cdot \end{pmatrix}, \quad (\text{B1})$$

with the constraint  $|P(z)|^2 + |Q(z)|^2 = 1$  on the unit circle. Several methods can be used to find  $Q(z)$ ; four of the most common are via optimization, via root-finding, via Prony's method and recently proposed exact expression using contour integration [47].

The optimization-based technique, which was used by the original GQSP authors [33], begins by applying a Fourier transform to the condition  $|P(z)|^2 + |Q(z)|^2 = 1$ . Denoting by  $\vec{a}$  and  $\vec{b}$  the coefficient vectors of  $P(z)$  and  $Q(z)$  respectively, one obtains

$$\vec{a} \star \text{reverse}(\vec{a})^* + \vec{b} \star \text{reverse}(\vec{b})^* = \vec{\delta}. \quad (\text{B2})$$

One can then solve

$$\arg \min_b \left\| \vec{a} \star \text{reverse}(\vec{a})^* + \vec{b} \star \text{reverse}(\vec{b})^* - \vec{\delta} \right\|^2. \quad (\text{B3})$$

to find a suitable  $\vec{b}$ . Although straightforward to implement, this method can be sensitive to initial guesses and may suffer from limited numerical stability.

A more direct approach uses polynomial properties in the complex plane [48]. One first defines

$$g(z) = 1 - |P(z)|^2. \quad (\text{B4})$$

Half of the roots of  $g(z)$  lie inside the unit circle, while the other half lie outside. Let  $\{\xi_j\}$  be the roots within the unit circle. Then a polynomial  $Q(z)$  satisfying  $|Q(z)|^2 = g(z)$  on  $|z| = 1$  can be written up to scaling as

$$Q(z) \propto \prod_{|\xi_j| < 1} (z - \xi_j). \quad (\text{B5})$$

Although conceptually simpler, this requires finding all the roots of a potentially high-degree polynomial, making it computationally expensive.

To address the scaling challenges of root finding, Prony's method was proposed in [44, 49]. Define

$$h(z) = \frac{1}{g(z)} = \frac{1}{1 - |P(z)|^2}. \quad (\text{B6})$$

In this formulation, the roots of  $g(z)$  become poles of  $h(z)$ . Hence  $h(z)$  can be expressed as

$$h(z) = \sum_{\xi_j} \frac{c_j}{z - \xi_j} + \text{constant} \quad (\text{B7})$$

Next, one computes the Fourier coefficients  $\hat{h}_k$  of  $h(z)$ :

$$\hat{h}_k = \frac{1}{2\pi i} \int_{\gamma} \frac{h(z)}{z^k} \frac{dz}{z} = - \sum_{|\xi_j| < 1} c_j \xi_j^{-(k+1)}, \quad (\text{B8})$$

where  $\gamma$  is the unit circle. Thus, each  $\hat{h}_k$  is a linear combination of the inverses of the roots inside  $\gamma$ . By following Prony's approach, the polynomial for  $Q(z)$  emerges from solving

$$\begin{pmatrix} \hat{h}_{-1} & \hat{h}_{-2} & \cdots & \hat{h}_{-(d+1)} \\ \hat{h}_{-2} & \hat{h}_{-3} & \cdots & \hat{h}_{-(d+2)} \\ \vdots & \vdots & \ddots & \vdots \\ \hat{h}_{-l} & \hat{h}_{-l+1} & \cdots & \hat{h}_{-(d+l)} \end{pmatrix} \begin{pmatrix} m_0 \\ m_1 \\ \vdots \\ m_d \end{pmatrix} = 0. \quad (\text{B9})$$

The coefficients  $m_j$  of  $Q(z)$  up to a scaling factor can be obtained via the singular value decomposition (SVD). In particular, if  $H_{\text{prony}}$  is the above matrix, its SVD is  $H_{\text{prony}} = U_{\text{SVD}} \Sigma V_{\text{SVD}}^\dagger$ . Because  $\text{rank}(H_{\text{prony}}) < d + 1$ ,  $\Sigma$  has at least one zero and the corresponding column of  $V_{\text{SVD}}$  supplies  $\vec{m}$ .

The most advanced technique for the completion step, also relying on complex analysis, was introduced in [47]. In this approach, we begin with the function  $g(z)$  defined in equation B4, but this time we apply logarithm:

$$w(z) = \log(g(z)). \quad (\text{B10})$$

Next, we calculate the Fourier series of the boundary function  $w(e^{i\theta})$ , denoted by  $\hat{w}(\theta)$ . We then apply projection operator  $\Pi$ , which leaves only non-negative frequency components from  $\hat{w}(\theta)$  and halves the constant

term:

$$\Pi[e^{in\theta}] := \begin{cases} e^{in\theta}, & n \in \mathbb{Z}_{>0}, \\ \frac{1}{2}, & n = 0, \\ 0, & n \in \mathbb{Z}_{<0}. \end{cases} \quad (\text{B11})$$

That projection ensures that  $\Pi w(z)$  is holomorphic inside the unit disc, and thus the resulting polynomial  $Q(z)$  will contain only non-negative powers of  $z$ .

Finally, we recover the polynomial  $Q(z)$  by exponentiating the projected function:

$$Q(z) = \exp[\Pi w(z)]. \quad (\text{B12})$$

After completing  $P(U)$  and  $Q(U)$ , the final step is called carving, in which the GQSP sequence (see Eq. 3) is unwrapped from the end:

$$\begin{pmatrix} \hat{P}(U) & \cdot \\ \hat{Q}(U) & \cdot \end{pmatrix} = CU^\dagger R(\theta_j, \phi_j, 0)^\dagger \begin{pmatrix} P(U) & \cdot \\ Q(U) & \cdot \end{pmatrix} = \begin{pmatrix} e^{-i\phi_j} \cos(\theta_j) U^\dagger & \sin(\theta_j) U^\dagger \\ e^{-i\phi_j} \sin(\theta_j) I & -\cos(\theta_j) I \end{pmatrix} \begin{pmatrix} P(U) & \cdot \\ Q(U) & \cdot \end{pmatrix}, \quad (\text{B13})$$

yielding new polynomials  $\hat{P}(U)$  and  $\hat{Q}(U)$  of one degree lower than  $P(U)$  and  $Q(U)$ . At each iteration, we extract the rotation angles via

$$\begin{aligned} \theta_j &= \tan^{-1} \left( \frac{|b_j|}{|a_j|} \right), \\ \phi_j &= \arg \left( \frac{a_j}{b_j} \right), \\ \lambda_0 &= \arg(b_0) \end{aligned} \quad (\text{B14})$$

The process is repeated until the sequence is fully carved out; any remaining global phase is stored in the final angle  $\lambda_0$ .

In practice, numerical problems may arise when  $P(z)$  has nearly zero coefficients for high or low powers. This can reduce the numerical rank of  $H_{\text{prony}}$  in B9. To mitigate this, a *capitalization* technique is used, where one adds and subtracts an auxiliary polynomial  $P'(z)$  with large coefficients at the highest and lowest powers:

$$P''(z) = \frac{1}{\beta} P(z) - P'(z) = \frac{1}{\beta} P(z) - \gamma(z^d + 1), \quad (\text{B15})$$

where  $\beta$  and  $\gamma$  are suitably chosen large constants. Then we work with  $P''(z)$ , which is numerically more stable.

Once  $P''(U)$  is computed, we must recover  $P(U)$ . This requires adding back  $P'(U)$  using an extra qubit, as shown in Fig. 11:

Although this method doubling the circuit depth and consumes an additional qubit, it stabilizes the numerical procedure.

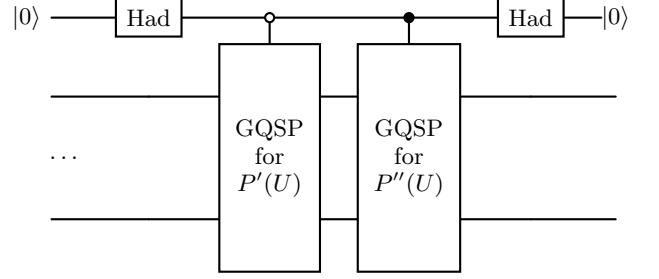


FIG. 11: Quantum circuit to restore the original polynomial  $P(U)$  after the capitalization step, using LCU with one additional qubit.

### Appendix C: Comparison of QII with Q-Inv and I-Iter for different truncation

Here we present analysis of how the convergence behavior of QII changes with different truncations of the Taylor polynomial. As a general rule, the convergence limit depends on the truncation: the higher the polynomial degree, the lower the energy.

For  $\text{H}_2$  QII achieves chemical accuracy for all tested values  $n$ . Q-Inv( $n = 1$ ) goes very closely to QII( $n = 5$ ). Curves for QII( $n = 20$ ), QII( $n = 50$ ), I-Iter( $n = 1$ ) and Q-Inv+I-Iter( $n = n_{\text{eq}}$ ) grouped near  $4 * 10^{-16}$ , which is the most likely consequence of machine precision.

For LiH, the polynomial truncation in QII becomes a more significant constraint. The chemical accuracy is achieved only for  $n \geq 20$ , while the lower  $n$  values converge to energies above the chemical accuracy. However, once  $n$  is large enough, QII converges faster than Q-Inv and I-Iter: QII( $n = 20$ ) requires just two iterations to reach chemical accuracy, while QII( $n = 50$ ) does so in a single iteration.

A similar trend appears for  $\text{BeH}_2$ . QII with  $n \geq 20$  achieves chemical accuracy with seven iterations at  $n = 20$  and just one iteration at  $n = 50$ . Again, QII( $n = 50$ ) initially converges faster than I-Iter or Q-Inv. However, after about 30 iterations, the combined Q-Inv+I-Iter approach slightly overtakes QII( $n = 50$ ). Extending QII to  $n > 50$  can further improve its final accuracy.

The ground state of the square  $\text{H}_4$  system exhibits a strong multireference character, making it the most challenging case. Only QII( $n = 50$ ) achieves chemical accuracy, doing so in just two iterations. However, at longer iteration counts (beyond 10), I-Iter eventually reaches lower energies. As before, increasing the degree of polynomial  $n$  in QII could further enhance its performance. In contrast, the Q-Inv method alone does not achieve the chemical accuracy of this system within the tested iterations.

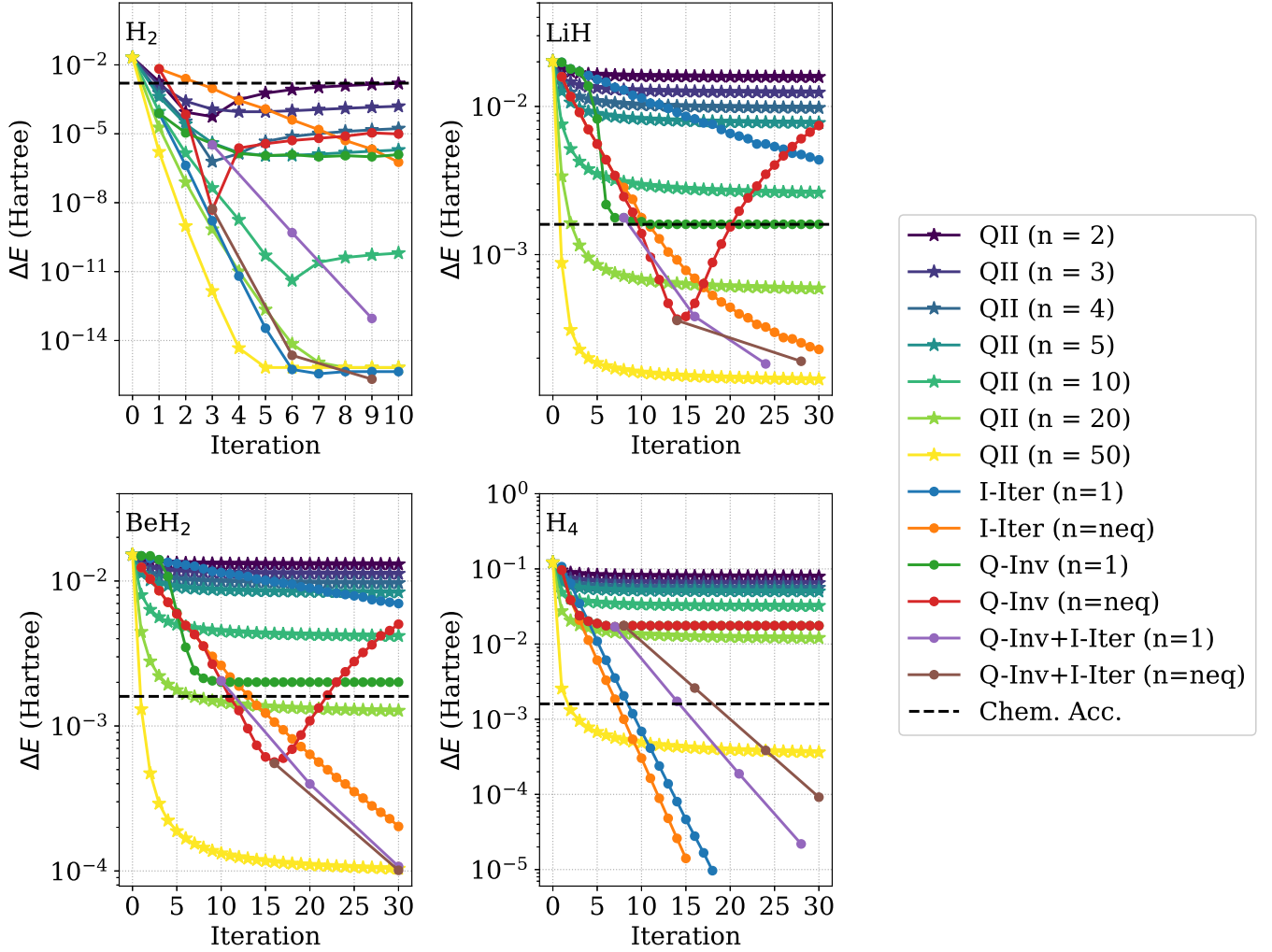


FIG. 12: Comparison of QII, I-Iter, and Q-Inv [27] for  $H_2$ ,  $LiH$ ,  $BeH_2$ , and  $H_4$ . Shown is the deviation from CASCI energies as a function of the iteration number. For QII,  $n$  refers to the polynomial truncation degree, while for I-Iter and Q-Inv,  $n$  is the Gauss-Legendre polynomial order.  $n_{eq}$  is the order at which energy convergence is reached.

- [1] B. Bauer, S. Bravyi, M. Motta, and G. K.-L. Chan, Quantum algorithms for quantum chemistry and quantum materials science, *Chem. Rev.* **120**, 12685 (2020).
- [2] M. Motta and J. E. Rice, Emerging quantum computing algorithms for quantum chemistry, *WIREs Comput. Mol. Sci.* **12**, e1580 (2022).
- [3] S. Lloyd, Universal quantum simulators, *Science* **273**, 1073 (1996).
- [4] A. Aspuru-Guzik, A. D. Dutoi, P. J. Love, and M. Head-Gordon, Simulated quantum computation of molecular energies, *Science* **309**, 1704 (2005).
- [5] Z. Ding and L. Lin, Even shorter quantum circuit for phase estimation on early fault-tolerant quantum computers with applications to ground-state energy estimation, *PRX Quantum* **4**, 020331 (2023).
- [6] L. Lin and Y. Tong, Heisenberg-limited ground-state energy estimation for early fault-tolerant quantum computers, *PRX Quantum* **3**, 010318 (2022).
- [7] A. Peruzzo, J. McClean, P. Shadbolt, M.-H. Yung, X.-Q. Zhou, P. J. Love, A. Aspuru-Guzik, and J. L. O'Brien, A variational eigenvalue solver on a photonic quantum processor, *Nat. Commun.* **5**, 4213 (2014).
- [8] A. G. Taube and R. J. Bartlett, New perspectives on unitary coupled-cluster theory, *Int. J. Quantum Chem.* **106**, 3393 (2006).
- [9] A. Kandala, A. Mezzacapo, K. Temme, M. Takita, M. Brink, J. M. Chow, and J. M. Gambetta, Hardware-efficient variational quantum eigensolver for small molecules and quantum magnets, *Nature* **549**, 242 (2017).
- [10] A. J. McCaskey, Z. P. Parks, J. Jakowski, S. V. Moore, T. D. Morris, T. S. Humble, and R. C. Pooser, Quantum chemistry as a benchmark for near-term quantum computers, *npj Quantum Inf.* **5**, 99 (2019).

- [11] S. Wang, E. Fontana, M. Cerezo, K. Sharma, A. Sone, L. Cincio, and P. J. Coles, Noise-induced barren plateaus in variational quantum algorithms, *Nat. Commun.* **12**, 6961 (2021).
- [12] M. Motta, C. Sun, A. T. K. Tan, M. J. O'Rourke, E. Ye, A. J. Minnich, F. G. S. L. Brandão, and G. K.-L. Chan, Determining eigenstates and thermal states on a quantum computer using quantum imaginary time evolution, *Nat. Phys.* **16**, 205 (2020).
- [13] S. McArdle, T. Jones, S. Endo, Y. Li, S. C. Benjamin, and X. Yuan, Variational ansatz-based quantum simulation of imaginary time evolution, *npj Quantum Information* **5**, 75 (2019).
- [14] H.-E. Li, X. Li, J.-C. Huang, G.-Z. Zhang, Z.-P. Shen, C. Zhao, J. Li, and H.-S. Hu, Variational quantum imaginary time evolution for matrix product state ansatz with tests on transcorrelated hamiltonians, *The Journal of Chemical Physics* **161**, 144104 (2024).
- [15] X. Yi, J. Huo, G. Liu, L. Fan, R. Zhang, and C. Cao, A probabilistic quantum algorithm for imaginary-time evolution based on taylor expansion, *EPJ Quantum Technology* **12**, 43 (2025).
- [16] I. Kolotouros, D. Joseph, and A. K. Narayanan, Accelerating quantum imaginary-time evolution with random measurements, *Phys. Rev. A* **111**, 012424 (2025).
- [17] H. H. S. Chan, D. M. Ramo, and N. Fitzpatrick, Simulating non-unitary dynamics using quantum signal processing with unitary block encoding, *arXiv preprint arXiv:2303.06161* (2023).
- [18] Y. Ge, J. Tura, and J. I. Cirac, Faster ground state preparation and high-precision ground energy estimation with fewer qubits, *J. Math. Phys.* **60**, 022202 (2019).
- [19] K. Seki and S. Yunoki, Quantum power method by a superposition of time-evolved states, *PRX Quantum* **2**, 010333 (2021).
- [20] B. C. Britt, Quantum power iteration to efficiently obtain the dominant eigenvector from diagonalizable nonnegative matrices, *Quantum Inf. Process.* **23**, 36 (2024).
- [21] A. W. Harrow, A. Hassidim, and S. Lloyd, Quantum algorithm for linear systems of equations, *Phys. Rev. Lett.* **103**, 150502 (2009).
- [22] N. A. Nghiem and T.-C. Wei, Quantum algorithm for estimating largest eigenvalues, *Physics Letters A* **488**, 129138 (2023).
- [23] A. Gilyén, Y. Su, G. H. Low, and N. Wiebe, Quantum singular value transformation and beyond: exponential improvements for quantum matrix arithmetics, in *Proc. 51st ACM SIGACT Symp. Theory Comput. (STOC)* (2019) pp. 193–204.
- [24] T. Ko, H. Park, and S. Choi, Quantum random power method for ground state computation, *arXiv preprint arXiv:2408.08556* (2024).
- [25] N. A. Nghiem, H. Sukeno, S. Zhang, and T.-C. Wei, Improved quantum power method and numerical integration using a quantum singular-value transformation, *Phys. Rev. A* **111**, 012434 (2025).
- [26] O. Kyriienko, Quantum inverse iteration algorithm for programmable quantum simulators, *npj Quantum Inf.* **6**, 7 (2020).
- [27] M. Cainelli, R. Baba, and Y. Kurashige, Numerical investigation of the quantum inverse algorithm on small molecules, *J. Chem. Theory Comput.* **20**, 7855 (2024).
- [28] A. M. Childs, R. Kothari, and R. D. Somma, Quantum algorithm for systems of linear equations with exponentially improved dependence on precision, *SIAM J. Comput.* **46**, 1920 (2017).
- [29] T. Yoshikura, S. L. Ten-no, and T. Tsuchimochi, Quantum inverse algorithm via adaptive variational quantum linear solver: Applications to general eigenstates, *J. Phys. Chem. A* **127**, 6577 (2023).
- [30] M. Motta, W. Kirby, I. Liepuoniute, K. J. Sung, J. Cohn, A. Mezzacapo, K. Klymko, N. Nguyen, N. Yoshioka, and J. E. Rice, Subspace methods for electron. struct. simulations on quantum computers, *Electron. Struct.* **6**, 013001 (2024).
- [31] N. H. Stair, R. Huang, and F. A. Evangelista, A multireference quantum krylov algorithm for strongly correlated electrons, *J. Chem. Theory Comput.* **16**, 2236 (2020).
- [32] N. Yoshioka, M. Amico, W. Kirby, P. Jurcevic, A. Dutt, B. Fuller, S. Garion, H. Haas, I. Hamamura, A. Ivrii, R. Majumdar, Z. Mineev, M. Motta, B. Pokharel, P. Rivero, K. Sharma, C. J. Wood, A. Javadi-Abhari, and A. Mezzacapo, Krylov diagonalization of large many-body Hamiltonians on a quantum processor, *Nature Communications* **16**, 5014 (2025).
- [33] D. Motlagh and N. Wiebe, Generalized quantum signal processing, *PRX Quantum* **5**, 020368 (2024).
- [34] C. Sünderhauf, Generalized quantum singular value transformation, *arXiv preprint arXiv:2312.00723* (2023).
- [35] L. Cadi Tazi and A. J. W. Thom, Folded spectrum vqe: A quantum computing method for the calculation of molecular excited states, *Journal of Chemical Theory and Computation* **20**, 2491 (2024).
- [36] G. H. Low and I. L. Chuang, Optimal hamiltonian simulation by quantum signal processing, *Phys. Rev. Lett.* **118**, 010501 (2017).
- [37] G. H. Low and I. L. Chuang, Hamiltonian Simulation by Qubitization, *Quantum* **3**, 163 (2019).
- [38] Y. C. Chen and T. K. Lee, t-j model studied by the power lanczos method, *Phys. Rev. B* **51**, 6723 (1995).
- [39] Q. Sun, X. Zhang, S. Banerjee, P. Bao, M. Barbry, N. S. Blunt, N. A. Bogdanov, G. H. Booth, J. Chen, Z.-H. Cui, J. J. Eriksen, Y. Gao, S. Guo, J. Hermann, M. R. Hermes, K. Koh, P. Koval, S. Lehtola, Z. Li, J. Liu, N. Mardirossian, J. D. McClain, M. Motta, B. Mussard, H. Q. Pham, A. Pulkin, W. Purwanto, P. J. Robinson, E. Ronca, E. R. Sayfutyarova, M. Scheurer, H. F. Schurkus, J. E. T. Smith, C. Sun, S.-N. Sun, S. Upadhyay, L. K. Wagner, X. Wang, A. White, J. D. Whitfield, M. J. Williamson, S. Wouters, J. Yang, J. M. Yu, T. Zhu, T. C. Berkelbach, S. Sharma, A. Y. Sokolov, and G. K.-L. Chan, Recent developments in the PySCF program package, *J. Chem. Phys.* **153**, 024109 (2020).
- [40] T. Tsuchimochi, Y. Mori, Y. Shimomoto, T. Nishimaki, Y. Ryo, M. Taii, T. Yoshikura, S. C. Tsang, K. Sasasako, and K. Yoshimura, Quket: Quantum unified kernel for emulator toolbox, <https://github.com/quket/quket> (2022).
- [41] S. Bravyi, J. M. Gambetta, A. Mezzacapo, and K. Temme, Tapering off qubits to simulate fermionic hamiltonians, *arXiv preprint arXiv:1701.08213* (2017).
- [42] K. Setia, R. Chen, J. E. Rice, A. Mezzacapo, M. Pistoia, and J. D. Whitfield, Reducing qubit requirements for quantum simulations using molecular point group symmetries, *J. Chem. Theory Comput.* **16**, 6091 (2020).
- [43] Y. Suzuki, Y. Kawase, Y. Masumura, Y. Hiraga, M. Nakadai, J. Chen, K. M. Nakanishi, K. Mitarai, R. Imai, S. Tamiya, T. Yamamoto, T. Yan, T. Kawakubo,



- Y. O. Nakagawa, Y. Ibe, Y. Zhang, H. Yamashita, H. Yoshimura, A. Hayashi, and K. Fujii, Qulacs: a fast and versatile quantum circuit simulator for research purpose, *Quantum* **5**, 559 (2021).
- [44] S. Yamamoto and N. Yoshioka, Robust angle finding for generalized quantum signal processing, *arXiv preprint arXiv:2402.03016* (2024).
- [45] L. Cadi Tazi and A. J. W. Thom, Folded spectrum vqe: A quantum computing method for the calculation of molecular excited states, *J. Chem. Theory Comput.* **20**, 2491 (2024).
- [46] A. M. Childs and N. Wiebe, Hamiltonian simulation using linear combinations of unitary operations, *Quantum Inf. Comput.* **12** (2012).
- [47] B. K. Berntson and C. Sünderhauf, Complementary polynomials in quantum signal processing, *arXiv preprint arXiv:2406.04246* (2024).
- [48] R. Chao, D. Ding, A. Gilyen, C. Huang, and M. Szegedy, Finding angles for quantum signal processing with machine precision, *arXiv preprint arXiv:2003.02831* (2020).
- [49] L. Ying, Stable factorization for phase factors of quantum signal processing, *Quantum* **6**, 842 (2022).